Received: 25 April 2024 | Revised: 23 January 2025 | Accepted: 26 January 2025

DOI: 10.1002/cac2.70004

CANCER COMMUNICATIONS Open Access

ORIGINAL ARTICLE

Helicobacter pylori CagA elevates FTO to induce gastric cancer progression via a "hit-and-run" paradigm

Bing He[1] | **Yiyang Hu**[2] | **Yuyun Wu**[1] | **Chao Wang**[1] | **Limin Gao**[1] | **Chunli Gong**[1] | **Zhibin Li**[1] | **Nannan Gao**[1] | **Huan Yang**[1] | **Yufeng Xiao**[1] | **Shiming Yang**[1,3]

[1]Department of Gastroenterology, Xinqiao Hospital, Army Military Medical University, Chongqing, P. R. China

[2]Department of Oncology, The General Hospital of Western Theater Command, Chengdu, Sichuan, P. R. China

[3]Chongqing Institute for Brain and Intelligence, Guangyang Bay Laboratory, Chongqing, P. R. China

Correspondence
Shiming Yang, Department of Gastroenterology, Xinqiao Hospital, Army Military Medical University, Chongqing, P. R. China.
Email: yangshiming@tmmu.edu.cn

Yufeng Xiao, Department of Gastroenterology, Xinqiao Hospital, Army Military Medical University, Chongqing, P. R. China.
Email: xiaoyufeng@tmmu.edu.cn

Funding information
National Natural Science Foundation of China, Grant/Award Number: No. 82203479; The Key Program of Natural Science Foundation of Chongqing, Grant/Award Number: No. cstc2020jcyj-zdxmX0020; Natural Science

Abstract

Background: *Helicobacter pylori* (*H. pylori*) infection contributes significantly to gastric cancer (GC) progression. The intrinsic mechanisms of *H. pylori*-host interactions and their role in promoting GC progression need further investigation. In this study, we explored the potential role of fat mass and obesity-associated protein (FTO) in mediating Cytotoxin-associated gene A (CagA)-induced GC progression.

Methods: The effects of *H. pylori* infection on N^6-methyladenosine (m^6A) modification were evaluated in both human samples and GC cell lines. The function of FTO in the progression of GC was elucidated through in vitro and in vivo studies. A series of techniques, including methylated RNA immunoprecipitation sequencing, RNA sequencing, RNA binding protein immunoprecipitation, and chromatin immunoprecipitation assays, were utilized to investigate the mechanism by which FTO mediates the capacity of *cagA*-positive *H. pylori* to promote GC progression. Furthermore, the therapeutic potential of the FTO inhibitor

Abbreviations: BSA, bovine serum albumin; CagA, cytotoxin-associated gene A; CEA, carcinoembryonic antigen; ChIP, chromatin immunoprecipitation; CK20, cytokeratin 20; CK7, cytokeratin 7; DAPI, 4',6-diamidino-2-phenylindole; DMSO, Dimethyl sulfoxide; DOX, doxycycline; E-Ca, E-cadherin; EMT, epithelial-mesenchymal transition; EpCAM, epithelial cell adhesion molecule; FBS, Fetal bovine serum; FDA, Food and Drug Administration; FTO, fat mass and obesity-associated protein; GAPDH, Glyceraldehyde 3-phosphate dehydrogenase; GC, gastric cancer; GEO, Gene Expression Omnibus; GO, Gene Ontology; GSEA, Gene enrichment set analysis; GSVA, Gene Set Variation Analysis; H. pylori, Helicobacter pylori; HBEGF, heparin-binding EGF like growth factor; HE, hematoxylin and eosin stain; IHC, immunohistochemistry; JASPAR, Journal of A Comprehensive Source of Promoter Analysis and Recognition; JUN, Jun Proto-Oncogene; KEGG, Kyoto Encyclopedia of Genes and Genomes; Kna, kanamycin; m6A, N6-methyladenosine; m6A-IP, Methylated RNA immunoprecipitation; MA, meclofenamic acid; MAPK, mitogen-activated protein kinase; MB, Methylene blue stain; MeRIP, methylated RNA immunoprecipitation; MOI, multiplicity of infection; MS, mass spectrometry; mut, Mutant; N-Ca, N-cadherin; OS, overall survival; PBS, phosphate buffered solution; PSA, periodic acid-schiff; RIP, RNA Immunoprecipitation; shRNA, short hair RNA; TCGA, The Cancer Genome Atlas; TFDB, the Animal Transcription Factor DataBase; TFs, transcription factors; TMA, tissue microarray; Vim, Vimentin; WT, Wide Type; YTHDF2, YTH N(6)-methyladenosine RNA binding protein 2.

Bing He, Yiyang Hu, Yuyun Wu, and Chao Wang contributed equally to this work.

Foundation of Chongqing, Grant/Award Number: No. CSTB2023NSCQ-MSX0408

meclofenamic acid (MA) in impeding GC progression was evaluated across GC cells, animal models, and human GC organoids.

Results: Infection with *cagA*-positive *H. pylori* upregulated the expression of *FTO*, which was essential for CagA-mediated GC metastasis and significantly associated with a poor prognosis in GC patients. Mechanistically, CagA delivered by *H. pylori* enhanced *FTO* transcription via Jun proto-oncogene. Elevated FTO induced demethylation of m^6A and inhibited the degradation of heparin-binding EGF-like growth factor (HBEGF), thereby facilitating the epithelial-mesenchymal transition (EMT) process in GC cells. Interestingly, eradication of *H. pylori* did not fully reverse the increases in FTO and HBEGF levels induced by *cagA*-positive *H. pylori*. However, treatment with a combination of antibiotics and MA substantially inhibited *cagA*-positive *H. pylori*-induced EMT and prevented GC metastasis.

Conclusion: Our study revealed that FTO mediates the "hit-and-run" mechanism of CagA-induced GC progression, which suggests that the therapeutic targeting of FTO could offer a promising approach to the prevention of CagA-induced cancer progression.

KEYWORDS
Epithelial-Mesenchymal transition, FTO, Gastric cancer, *Helicobacter pylori*, m^6A modification

1 | BACKGROUND

Gastric cancer (GC) ranks as the fifth most prevalent malignant tumor and is the fourth leading cause of cancer-related death [1, 2]. Chronic infection with *Helicobacter pylori* (*H. pylori*) is a significant contributor to the development of GC [3, 4]. The pathohistological outcome of *H. pylori* infection is influenced by both the bacterium's virulence factors and the host's genetic characteristics [5, 6]. Among these virulence factors, cytotoxin-associated gene A (CagA) stands out as the primary factor, which can be delivered into host cells via the type IV secretion system (T4SS), thereby triggering a cascade of oncogenic signaling pathways [7–10]. Strains of *H. pylori* that harbor the *cagA* gene ($cagA^+$) are associated with more pronounced gastric mucosal damage and exhibit a higher propensity for inducing GC compared to *cagA*-negative strains [6, 7, 11].

Given the prominent role of *H. pylori* in the progression of GC, strategies for large-scale screening and eradication of *H. pylori* have been implemented with the aim of preventing and treating GC [1, 12]. A wealth of prospective studies and meta-analyses have demonstrated that the eradication of *H. pylori* is associated with a reduced risk of GC [12–15]. Nevertheless, pathohistological findings suggest that successful eradication of *H. pylori* failed to prevent the development of GC [16, 17]. Infection with $cagA^+$ *H. pylori* can elicit genomic and epigenetic alterations in host cells that may perpetuate tumor progression even in the absence of the pathogen [18]. Consequently, CagA is hypothesized to mediate carcinogenesis through a "hit-and-run" mechanism [18, 19], although the precise mechanism underlying this process is not yet fully understood.

N^6-methyladenosine (m^6A) modification is a dynamic process that modulates gene expression in response to environmental stimuli [20–22] and plays an essential role in the development of tumors [23–26]. Hence, we proposed the hypothesis that infection with $cagA^+$ *H. pylori* induces irreversible alterations in host cell m^6A methylation, thereby facilitating GC progression in a "hit-and-run" manner. To validate this hypothesis, we conducted a series of investigations to delineate the role and underlying molecular mechanisms of m^6A methylation in $cagA^+$ *H. pylori* infection. Furthermore, we assessed the therapeutic efficacy of specific m^6A small-molecule inhibitors in impeding GC progression.

2 | MATERIALS AND METHODS

2.1 | Cell and *H. pylori* culture

MKN45 and AGS cell lines were obtained from the Japanese Collection of Research Bioresources (Osaka,

Japan) and the American Type Culture Collection (Manassas, VA, USA), respectively. The cells were cultivated in Dulbecco's Modified Eagle Medium (#C11965500BT, Gibco, Burlington, MA, USA) supplemented with 10% fetal bovine serum (FBS, #A5669701, Gibco). All of the cell lines were confirmed by genotyping and were tested regularly for mycoplasma contamination.

The *H. pylori* wild-type (*WT*) *cagA*$^+$ strain (National Collection of Type Cultures [NCTC] 11637, *cagA*$^+$ *H. pylori*) and *H. pylori* isogenic mutant strain (NCTC 11637*ΔcagA*, *ΔcagA H. pylori*) were provided by Professor Quanming Zou and Yuan Zhuang, who come from Army Military Medical University (Chongqing, P. R. China). The strains were inoculated onto *H. pylori* culture plates enriched with 5% sheep blood (#HB8646, HOPEBIO, Qingdao, Shandong, P. R. China) and incubated at 37°C under microaerobic conditions (10% CO_2, 5% O_2, 85% N_2), utilizing a microaerophilic system (Becton, Dickinson and Company, San Diego, CA, USA).

2.2 | Clinical tissue samples and organoid culture

Cancerous tissues were collected from fifteen patients with pathologically confirmed GC. The utilization of patient samples was approved by the Medical Ethics Committee of Xinqiao Hospital of Army Medical University (Approved No. 2024-083-01). Using an *H. pylori* antibody classification assay kit (#CP01, Blot, Shenzhen, Guangdong, P. R. China), we systematically categorized all patient samples into CagA-positive (n = 8) or CagA-negative (n = 7) groups. This classification was subsequently verified through immunohistochemical (IHC) detection of the CagA protein using CagA antibody (#sc-28368, Santa Cruz Biotech, Dallas, TX, USA). We also obtained RNA-seq data from GC patients in The Cancer Genome Atlas (TCGA) database, with the dataset project ID TCGA-STAD.

Fresh GC tissues were washed in phosphate-buffered saline (PBS) with 1% penicillin-streptomycin and cut into 1-3 mm^2 fragments. A digestion mixture was prepared with 10 mL of organoid culture medium (#K2179-GC, BioGenous, Suzhou, Zhejiang, P. R. China), 1 mg of collagenase XI (#C7657, Sigma Aldrich, Burlington, MA, USA) and 10 mg of dispase II (#D4693, Sigma Aldrich). The fragments underwent enzymatic digestion for about 1 hour. Gentle pipetting dispersed the fragments in PBS. Fragments were collected and resuspended in Matrigel (#356231, Corning, Bedford, NY, USA) at 50 μL per well, seeded into a prewarmed 24-well plate, and allowed to solidify at 37°C for 10 minutes. After solidification, 500 μL of complete organoid culture medium was added to each well. The medium was refreshed every two to three days. Three CagA-negative GC organoids were successfully cultured for further experiments.

2.3 | Co-culture of *H. pylori* with cells and organoids

GC cells at the logarithmic growth stage were seeded into 6-well plates and cultured in an antibiotic-free medium. *H. pylori* was then harvested and introduced into the GC cells at a multiplicity of infection (MOI) of 100:1. After 24 hours of co-culture, the GC cells were collected for further analysis.

We performed co-cultures of *H. pylori* with organoids as described in previously published literature [27]. Briefly, well-formed organoids were selected and centrifuged at 300 ×*g* for 5 minutes. The organoids were then resuspended in a culture medium and transferred to 15 mL tubes. *H. pylori* was scraped with an inoculation loop and suspended in 1 mL of sterile PBS. After centrifuging at 5000 rpm for 5 minutes, the bacteria were resuspended in 1 mL of sterile PBS. This suspension was then mixed with the organoids in a 15 mL tube and incubated for 3 hours. Thereafter, the organoids were resuspended in Matrigel and placed into individual wells of a 24-well plate. Each well was then filled with 500 μL of standard organoid culture medium.

2.4 | Tissue microarray (TMA) and IHC

Human GC TMAs with documented *H. pylori* infection status were purchased from Shanghai Outdo Biotech Co. Ltd. (#HStmA180Su30, Shanghai, P. R. China). This company has provided ethical approval for these TMAs (Approved No. YBM-05-02). The TMA includes cancerous tissues and their corresponding para-carcinoma counterparts from a cohort of 83 GC patients, supplemented by cancer tissues from 14 additional patients that lack matched para-carcinoma tissues. IHC was performed using a commercial IHC staining kit (# IHC001 and IHC003, Boster, Pleasanton, CA, USA), IHC staining strictly following the instructions. In brief, the TMAs were deparaffinized with xylene and antigenically repaired with sodium citrate and serum blocking. The arrays were then probed with primary antibodies specific for either fat mass and obesity-associated protein (FTO, Abcam, Cambridge, MA, USA; 1:100) or CagA (Santa Cruz Biotech, 1:100), with incubation overnight. Subsequently, the TMAs were exposed to the corresponding secondary antibodies for 1 hour. The 3,3'-Diaminobenzidine (DAB) was used for color development, and the resulting slides were photographed using an orthomicroscope (Nikon, Tokyo, Japan). The staining intensity

was quantified by measuring the integrated optical density of the slides with the aid of ImageJ software (National Institutes of Health, Bethesda, MD, USA).

2.5 | Animal models

All of the animal studies were conducted in compliance with protocols approved by the Laboratory Animal Welfare and Ethics Committee of Army Military Medical University (Approval No. AMUWEC20235107). Four-week-old male nude mice (#401, Vital River, Beijing, P. R. China) were housed in a Specific Pathogen Free (SPF) laboratory environment and randomly assigned to groups of *shNC*, *shFTO*, *NC*, *FTO-WT-oe*, *FTO-mut1-oe*, and *FTO-mut2-oe*. Following induction of anesthesia, the mice were intravenously inoculated with 5×10^6 GC cells via the tail vein. Bioluminescent imaging was performed four weeks post-inoculation to assess lung metastasis. D-luciferin potassium salt (#P1042, 150 mg/kg, Promega, Madison, WI, USA) was administered intraperitoneally, and after a 10-minute interval, bioluminescent signals were captured using Bruker Molecular Imaging Software (Bruker, Billerica, MA, USA). At the end of the study, all animals were humanely euthanized. Hematoxylin-eosin (HE) staining was performed to confirm the lung metastatic burden.

For in vivo therapeutic experiments, CagA-tet-on or negative control (NC-tet-on) GC cells were administered via the tail vein injection. The mice were orally administered doxycycline (DOX, 500 mg/kg once daily; #HY-N0565, MedChemExpress, Monmouth Junction, NJ, USA) and intraperitoneally injected with MA (50 mg/kg, once every 3 days, #HY-B1320, MedChemExpress) for 30 days. Bioluminescent imaging and HE staining were carried out at the end of the treatment regimen.

2.6 | Dot blotting

Total RNA was extracted from GC cells or tissues, and prepared RNA dilutions were subjected to a denaturation step at 95°C for three minutes. A Hybond-N^+ membrane (#RPN303B, Millipore, Billerica, MA, USA) was utilized for the immobilization of 2 μL of RNA. The RNA on the membrane was crosslinked using an ultraviolet crosslinker (Stratagene, Santa Clara, CA, USA) at an intensity of 1200 μJ for two rounds, each lasting about 25 to 50 seconds. Post crosslinking, the membranes were incubated with a 1% solution of bovine serum albumin (BSA) for 1 hour. m^6A antibody (#ab284130, Abcam, 1:1000) and appropriate secondary antibodies were subsequently applied to the membranes at recommended dilution ratios. The enhanced chemiluminescence reagent (ECL, #P0018S, Beyotime, Shanghai, P. R. China) was prepared for luminescence detection. Membranes were photographed with the help of a chemiluminescence system (Bio-Rad, Hercules, CA, USA). To assess the total RNA content as a loading control, membranes were soaked for two hours in a 0.02% methylene blue solution (#S0296, Beyotime). Following this, membranes were rinsed with enzyme-free water, and images were captured with a camera.

2.7 | Organoid immunofluorescence and HE staining

Following the disposal of the media, organoids were washed twice with PBS. We used 4% paraformaldehyde to fix these organoids for 20 minutes at room temperature. After being softly trembling, the organoids were transferred to 1.5 mL centrifuge tubes. After which, samples were incubated with Triton-X 100 at 4°C for 30 minutes, treated with 1% BSA for 1 hour, and incubated with diluted primary and secondary antibodies at 4°C according to the manufacturer's directions. The antibodies used in this investigation are listed in Supplementary Table S1. Following a 10-minute at room temperature incubation period with 4',6-diamidino-2-phenylindole (DAPI), the organoids were washed with PBS. The organoids were then resuspended in 20 to50 μL of anti-fluorescence quenching sealing agent and examined under a microscope.

Characterization of organoids was achieved through HE and periodic acid-schiff (PAS) staining. For HE, the organoids were initially fixed in a 4% paraformaldehyde solution, followed by embedding in paraffin for sectioning. Sections were dehydrated with alcohol, stained with hematoxylin, rinsed, and treated with a bluing agent to enhance nuclear contrast. Eosin was then applied to stain cytoplasm and connective tissue. The slides were dehydrated, cleared, and mounted with neutral balsam for microscopic analysis. In the PAS process, the sections were oxidized with periodic acid to reveal glycogen. After rinsing away excess oxidizer, Schiff's reagent was applied for color development. The reaction was stopped with a wash, followed by counterstaining with hematoxylin to delineate cell nuclei. Finally, the slides were dehydrated, cleared, and mounted with neutral balsam for examination under a microscope.

2.8 | Plasmid construction

Lentiviral constructs overexpressing wild-type *FTO* and mutant *FTO* were generated as previously described [28]. Knockdown lentiviral plasmids, such as *shFTO* and *sh*

heparin-binding EGF-like growth factor (HBEGF), were cloned and integrated into the pPurGreen-shRNA lentiviral vector (#SI505A-1, System Biosciences, San Francisco, CA, USA) using the BamHI (# D6053, Beyotime) and EcoRI (#D6239, Beyotime) restriction enzymes. The target sequences for all *shRNAs* were detailed in Supplementary Table S2. The open reading frames (ORFs) of Flag-tagged Jun proto-oncogene (*JUN*), *HBEGF*, and *HBEGF-mut1/2* were amplified using the primers listed in Supplementary Table S3, with Flag tags incorporated during PCR and subsequently cloned into pCDH lentiviral vectors (#CD510B-1, System Biosciences) via EcoRI (#D6329, Beyotime) and NotI (#D6497, Beyotime) enzymatic sites. The coding sequence of the *cagA* gene from *cagA*$^+$ *H. pylori* RNA underwent reverse transcription, amplification, cloning, and was then inserted into tet-on lentiviral vectors (#030351, Clontech, Palo Alto, CA, USA), utilizing BamHI and EcoRI for the construction of CagA-tet-on lentiviral plasmids. All plasmid constructs were verified by DNA sequencing to ensure accuracy. The authenticated plasmids were co-transfected with packaging vectors psPAX2 (#12260, Addgene, Watertown, MA, USA) and pMD2.G (#12259, Addgene) into HEK293T cells to produce lentiviral particles, which were collected at 48 and 72 hours post-transfection. For establishing stable cell lines, GC cell lines MKN45 and AGS were transfected with the harvested virus in the presence of 4 μg/mL polybrene to enhance transduction efficiency.

2.9 | Western blotting

The cells and GC tissues were repeatedly washed with PBS, and protein extraction was obtained using radioimmunoprecipitation assay (RIPA) buffer (#P0013B, Beyotime). Protein concentration was quantified using a BCA Protein Assay Kit (#P0010, Beyotime). After sodium dodecyl sulfate-polyacrylamide gel electrophoresis (SDS-PAGE) separation, the proteins were transferred onto polyvinylidene fluoride (PVDF) membranes (Millipore). The membranes were then incubated with a blocking solution containing 5% BSA (#23210, Sangon, Shanghai, P. R. China) for 1 hour at room temperature. Following the step, membranes were incubated with primary antibodies, diluted according to the recommended ratios, and then with horseradish peroxidase (HRP)-conjugated secondary antibodies, as listed in Supplementary Table S1. After this, the membrane was uniformly treated with an appropriate amount of ECL reagent (#P0018S, Beyotime). Protein bands were then visualized with a chemiluminescence system (Bio-Rad). The intensity of the bands was quantitatively evaluated using ImageJ software.

2.10 | Quantitative real-time PCR (qRT-PCR)

RNAiso reagent (#9109, Takara, Kusatsu, Japan) was used for the extraction of total RNA from both tissue and cells. A PrimeScript™ RT Reagent Kit with gDNA Eraser (# RR047A, Takara) was used for reverse transcription. To evaluate RNA expression levels, qPCR was conducted using the SYBR® Premix Ex Taq Kit (# RR820A, Takara) according to the manufacturer's instructions. The relative expression of the target genes was calculated via the $2^{-\triangle\triangle CT}$ method, using glyceraldehyde-3-phosphate dehydrogenase (*GAPDH*) as the housekeeping gene [29]. Supplementary Table S4 lists the sequences of the primers used.

2.11 | RNA sequencing (RNA-Seq), Methylated RNA immunoprecipitation sequencing (MeRIP-seq) and MeRIP-qPCR

MeRIP-seq experiments were performed according to the procedure described in the literature [26]. Briefly, total RNA was extracted and purified, followed by denaturation and fragmentation into approximately 100-nt fragments. These RNA fragments were then incubated with protein A/G magnetic beads (#78609, Thermo Scientific, Waltham, MA, USA) in conjunction with an anti-m^{6}A antibody (#ab151230, Abcam). The input RNA and methylated RNA fragments, selectively bound to the m^{6}A antibody, were eluted and prepared for subsequent sequencing analysis (Unionchuan, Hangzhou, Zhejiang, P. R. China). Genes with a log2 Fold Change (FC) > 1 and $P < 0.01$ were identified as differentially expressed genes (DEGs). Genes with $P < 0.05$ were identified as m^{6}A-marked genes. Gene Ontology (GO) classification enrichment of DEGs was conducted using the Sangerbox database (http://sangerbox.com). GSVA analysis was performed via the Gene Set Cancer Analysis (GSCA) website (http://bioinfo.life.hust.edu.cn/GSCA/#/).

The specific m^{6}A sites in the mRNA of *HBEGF* were predicted using a sequence-based N6-methyladenosine (m^{6}A) modification site predictor, SRAMP (http://www.cuilab.cn/sramp). MeRIP-qPCR was performed to verify these predicted sites, employing a similar methodology to that of MeRIP-seq with certain procedural adaptations. Specifically, total RNA was fragmented into 200-nt pieces. Primers for PCR were custom-designed to target candidate sites of interest (Supplementary Table S5). The enrichment of RNA fragments bound to the m^{6}A antibody in each group was quantified via qRT-PCR. The input RNA served as an internal control for normalization.

2.12 | RNA immunoprecipitation (RIP)

A Magna RIP™ RNA Binding Protein Immunoprecipitation Kit (#17-700, Millipore) was used for the experiment. Briefly, the cell lysates were incubated at 4°C overnight with A/G magnetic beads (Millipore) in the presence of either an IgG control antibody or a YTH N(6)-methyladenosine RNA binding protein 2 (YTHDF2) (#24744-1-AP, Proteintech, Chicago, IL, USA) antibody. After being thoroughly washed, the A/G beads were harvested via a magnetic rack. RNA was then isolated, and qRT-PCR was performed to quantify the enrichment of HBEGF RNA associated with YTHDF2 or IgG antibodies.

2.13 | Identification of transcription factors (TFs) potentially interacting with FTO

The Animal TFDB (http://bioinfo.life.hust.edu.cn/AnimalTFDB/) and ChIP-Atlas (https://chip-atlas.org/) databases were used to identify TFs that may interact with the *FTO* promoter region. Further analysis of the correlation between the expression of these candidate TFs and *FTO* in our RNA-seq data from GC cells post-*cagA*$^+$ *H. pylori* infection was conducted. Additionally, the expression correlation of the candidate TFs and *FTO* in the data derived from Gene Expression Omnibus (GEO, accession ID: GSE62254, GSE26942, GSE15459, GSE84437) and TCGA-STAD cohort was assessed. TFs that can act on the FTO promoter and were associated with FTO expression were selected for further assessment. The JASPAR (https://jaspar.genereg.net/) and Animal TFDB databases were selected to further predict the binding sites of the screened TFs with the *FTO* promoter. Based on the predicted results, *FTO* promoter-specific primers were designed for subsequent analysis.

2.14 | Chromatin immunoprecipitation (ChIP) assay

A Pierce Magnetic ChIP Kit (#26157, Thermo Scientific) was used for examinations according to the instructions. Initially, cells from each group were fixed with a 1% formaldehyde solution, followed by crosslinking and sonication. A portion of the lysate, 10 μL, was reserved as an input control and stored at -20°C. The remaining lysate was then incubated with either a JUN-specific antibody or IgG antibody overnight at 4°C, each at a final concentration of 10 μg/mL. Subsequently, 20 μL of A/G beads was added to the mixture, which was gently agitated for 2 hours at 4°C. The protein-chromatin complexes were carefully eluted, and the associated DNA was extracted after thorough washing. The immunoprecipitated DNA was subsequently analyzed using *FTO* promoter-specific primers (Supplementary Table S6) to amplify the region of interest via PCR.

2.15 | Enzyme-linked immunosorbent assay (ELISA)

The concentration of HBEGF was quantified using an HBEGF ELISA Kit (#EK14428, Signalway Antibody, College Park, MD, USA) according to the manufacturer's instructions. In brief, 100 μL of diluted standards and samples were injected into corresponding plate wells. The plate was then sealed with paper and incubated at 37°C for 2 hours. After disposal of the liquid, 100 μL of detection reagent A's working solution was dispensed into each well. The plate was resealed and incubated for 1 hour at 37°C. Post incubation, the solution was removed, and each well was rinsed with 300 μL of the provided wash solution. This washing process was repeated a total of three times. Subsequently, 100 μL of detection reagent B's working solution was added to each well and incubated for 1 hour. Next, 90 μL of the substrate mixture was introduced to the wells and incubated for 15 to 25 minutes. The reaction was quenched by the immediate addition of 50 μL of stop solution. Finally, the quantitative assessment was conducted according to the absorbance at 450 nm with a microplate reader (Thermo Scientific).

2.16 | Migration and invasion assays

Assays for migration were performed utilizing 24-well Transwell plates with 8-μm pores (#3428, Corning). The upper layer of each chamber was loaded with 5×10^4 cells in the logarithmic phase of growth. The lower compartment was filled with 500 μL of complete growth media containing 10% FBS. The plates were incubated for 24 hours at 37°C in a 5% CO_2 atmosphere to allow cell migration. After being fixed with a 4% paraformaldehyde solution and stained with 1% crystal violet, the lower surface of the membrane was examined using a light microscope to quantify the number of migrated cells. For the invasion assay, precooled Matrigel (#354234, Corning) was equally applied to the upper layer of a chamber in 24-well Transwell plates. The instructions for the migration assay were followed for subsequent procedures.

2.17 | RNA stability assay

GC cells were plated in six-well plates and allowed to adhere for 24 hours, at which point this was designated as the 0-hour time point. Subsequently, one well was harvested, and 5 μg/mL actinomycin D (#A9415, Sigma Aldrich) was introduced to the remaining wells. At 2-, 4-, and 6-hour post-treatment, the cells from each time point were collected. Total RNA was extracted with RNAiso (#9109, Takara), and qRT-PCR was used to determine the quantity of remaining RNA.

2.18 | Dual-luciferase reporter assay

MKN45 cells were transiently transfected with *FTO* reporter (Sangon) in 24-well plates utilizing Lipo8000™ (#C0533, Beyotime). After a 4-hour post-transfection incubation period, the cells were infected with *H. pylori* at a MOI of 100:1 for 24 hours. Subsequently, the cells were washed with PBS and lysed for a dual-luciferase assay (#E1960, Promega, Madison, MI, USA). The reporter activities were quantified using a microplate reader (Thermo Scientific). For experiments involving CagA and JUN, MKN45 cells with *cagA* overexpression or *JUN* knockdown and their respective controls were also transfected with *FTO* reporter. The dual-luciferase activity assay was performed 24 hours later.

2.19 | RNA pull-down and mass spectrometry analysis

The biotin-labeled probe of HBEGF (GenePharma, Shanghai, P. R. China) was diluted to a concentration of 20 pmol. This probe was then mixed with the cell lysate and streptomycin-coated magnetic beads (#65001, Thermo Scientific). The mixture was incubated at 4°C overnight. After sufficient washing, the RNA and associated proteins were eluted from the beads. These eluted samples were then prepared for further analysis via immunoblotting and mass spectrometry.

2.20 | Bioinformatic analysis

RNA-seq data from 408 GC patients within the TCGA cohort (the dataset project ID: TCGA-STAD) and detailed clinical features and prognostic information of 388 patients were downloaded from the UCSC Xena database (http://xenabrowser.net) on October 21, 2022. Patients were categorized into high and low expression groups based on the median gene expression value. Overall survival (OS) from the date of diagnosis was evaluated using Kaplan-Meier curves and assessed with the log-rank test. Expression profiles from the GEO datasets (accession ID: GSE62254, GSE29272, GSE14210, https://www.ncbi.nlm.nih.gov/geo/) were selected to validate relevant results. High and low expression groups were determined based on the optimal cutoff values via Kaplan-Meier Plotter (http://kmplot.com/analysis/), and survival curves were subsequently generated. For gene set enrichment analysis (GSEA) analysis, GSEA software version 3.0 was obtained from the official website (http://software.broadinstitute.org/gsea/index.jsp). RNA-seq data from *FTO* knockdown GC cells, retrieved from the GEO dataset (accession ID: GSE178697), were selected for analysis. The c2.cp.kegg.v7.4.symbols.gmt gene set collection was downloaded from the Molecular Signatures Database (http://www.gsea-msigdb.org/gsea/downloads.jsp) to evaluate the enrichment of genes within relevant pathways.

The (epithelial-mesenchymal transition) EMT score was calculated as: EMT score = (Fn1 + Vim + Zeb1 + Zeb2 + Twist1 + Twist2 + Snai1 + Snai2 + Cdh2) - (Cldn4 + Cldn7 + Tjp3 + Muc1 + Cdh1) [35]. The correlation between FTO expression and EMT scores in GC tissues from the TCGA-STAD cohort was assessed. EMT-associated genes were downloaded from the EMTome database (http://www.emtome.org/). The correlation between HBEGF levels and the EMT score in the majority of tumor types was assessed via the EMTome database.

2.21 | Statistical analysis

GraphPad Prism (version 9.0) was utilized for statistical tests. The results were displayed as average values and standard deviations (SD). The significance of the variance between the two groups was evaluated using either paired or unpaired Student's *t*-test. The variances between multiple groups were evaluated using either one-way or two-way ANOVA. Pearson correlation tests were employed to assess the interrelations between *FTO*, *HBEGF*, and *YTHDF2* levels. Survival for every group of GC patients was determined through Kaplan-Meier curves and analyzed using the log-rank test. A *P* value below 0.05 was acknowledged as statistically significant.

3 | RESULTS

3.1 | *cagA*$^+$ *H. pylori* mediated m^{6}A modification and induced *FTO* expression

To determine the impact of *cagA*$^+$ *H. pylori* infection on m^{6}A modification, we conducted an analysis on global

m^{6}A levels in GC tissues. Our results demonstrated that CagA-positive GC samples exhibited significantly reduced global m^{6}A levels in mRNA compared to those CagA-negative samples (Figure 1A, Supplementary Figure S1A-C). This finding was further confirmed in vitro using GC cells. Cells infected with the wild-type (*WT*) *H. pylori* *cagA*$^+$ strain (*cagA*$^+$ *H. pylori*) displayed lower m^{6}A levels when compared with both uninfected cells and cells infected with *H. pylori* isogenic mutant strains lacking *cagA* (*ΔcagA H. pylori*) (Figure 1B-C).

m^{6}A modifications were subject to dynamic regulation by a suite of m^{6}A regulators [30, 31], with FTO exhibiting the most pronounced up-regulation in response to *cagA* overexpression (Supplementary Figure S1D). This trend was corroborated in our analysis of GC tissues, where *FTO* expression was significantly higher in CagA-positive GC tissues when compared to CagA-negative GC tissues (Figure 1D, Supplementary Figure S1E). Further in vitro studies revealed that both mRNA and protein levels of FTO were significantly higher in *cagA*$^+$ *H. pylori*-infected GC cells compared to the uninfected group (Mock) and the *ΔcagA H. pylori*-infected group (Figure 1E-F). Consistent with these findings, *FTO* levels were significantly greater in *H. pylori*-infected GC tissues in the TCGA-STAD cohort compared to *H. pylori*-uninfected GC tissues (Supplementary Figure S1F). To simulate the infection of *cagA*$^+$ *H. pylori* in the host environment, human GC organoids were cultured and characterized using HE and PAS staining (Supplementary Figure S1G). The successful construction of GC organoids was verified by the expression of common GC markers, including carcinoembryonic antigen (CEA), cytokeratin 20 (CK20), epithelial cell adhesion molecule (EpCAM) and cytokeratin 7 (CK7), through immunofluorescence (Supplementary Figure S1H). Organoids derived from CagA-negative GC tissues were selected for inoculation with *cagA*$^+$ *H. pylori*. Notably, infection with *cagA*$^+$ *H. pylori* led to a significant increase in *FTO* expression in GC organoids compared to the Mock and *ΔcagA H. pylori* infection groups (Figure 1G).

The expression of *FTO* in the TCGA-STAD cohort was conducted to explore its clinical implications in GC. Compared to normal gastric tissues, GC tissues presented a markedly higher increase in *FTO* expression (Figure 1H). Robust correlations were identified between elevated *FTO* mRNA levels and key clinicopathological features, including lymph node metastasis, distant metastasis, and tumor stage (Figure 1I). In addition, when compared with the other subtypes of GC, the genomically stable subtype, which is associated with a more aggressive disease phenotype [34], exhibited significantly elevated *FTO* expression levels (Supplementary Figure S1I). The OS of GC patients with high *FTO* expression was significantly lower than those of patients with low *FTO* expression in both the TCGA-STAD cohort and GEO datasets (Figure 1J, Supplementary Figure S1J). These observations collectively suggest that the upregulation of *FTO* expression, potentially mediated by *cagA*$^+$ *H. pylori* infection, may play a pivotal role in the accelerated progression of GC.

3.2 | Elevated FTO was necessary for CagA-induced GC metastasis

To explore the biological functions of CagA-induced FTO upregulation in GC progression, we retrieved RNA-seq data of *FTO* knockdown GC cells from the GEO dataset (GSE178697) [32]. KEGG enrichment analysis revealed that the knockdown of *FTO* led to significant alterations in gene expression profiles, with a pronounced enrichment of genes implicated in EMT-related processes, such as cell adhesion, cell polarity, and ECM-receptor interaction (Figure 2A). These findings hint at a potential role of FTO in the induction of EMT in GC cells, thereby possibly facilitating their metastatic ability. Analysis of the GC dataset GSE62254 revealed that *FTO* expression levels were significantly elevated in tissues from patients exhibiting distant metastasis (M1) compared with those without metastasis (M0) (Figure 2B). Furthermore, the metastatic and invasive capabilities of GC cells were considerably attenuated following *FTO* knockdown (Figure 2C-D, Supplementary Figure S2A-B). To verify the demethylase function of FTO, we constructed lentiviruses harboring wild-type (*WT*) and mutant (*FTO-mut1*/*FTO-mut2*) *FTO* sequences (Supplementary Figure S2C-D), as previously described [28], and established stable cell lines with these lentiviruses (Figure 2E, Supplementary Figure S2E). Our results indicated that, in contrast to the mutants, *FTO-WT-oe* significantly augmented GC cell metastasis and invasion (Figure 2F, Supplementary Figure S2F).

Additionally, we observed that the migratory and invasive capacities of MKN45 and AGS cells were substantially increased upon infection with *cagA*$^+$ *H. pylori* (Figure 2G, Supplementary Figure S2G). Importantly, the metastatic effects induced by *cagA*$^+$ *H. pylori* infection were mitigated by *FTO* knockdown (Figure 2G, Supplementary Figure S2G), suggesting that the enhancement of GC cell migration by *cagA*$^+$ *H. pylori* is FTO-dependent.

3.3 | CagA transcriptionally promoted *FTO* expression through JUN

We have previously demonstrated that CagA was capable of elevating both mRNA and protein levels of *FTO* (Figure 1E-F). Furthermore, *cagA*$^+$ *H. pylori* infection did not influence mRNA stability (Figure 3A) but markedly

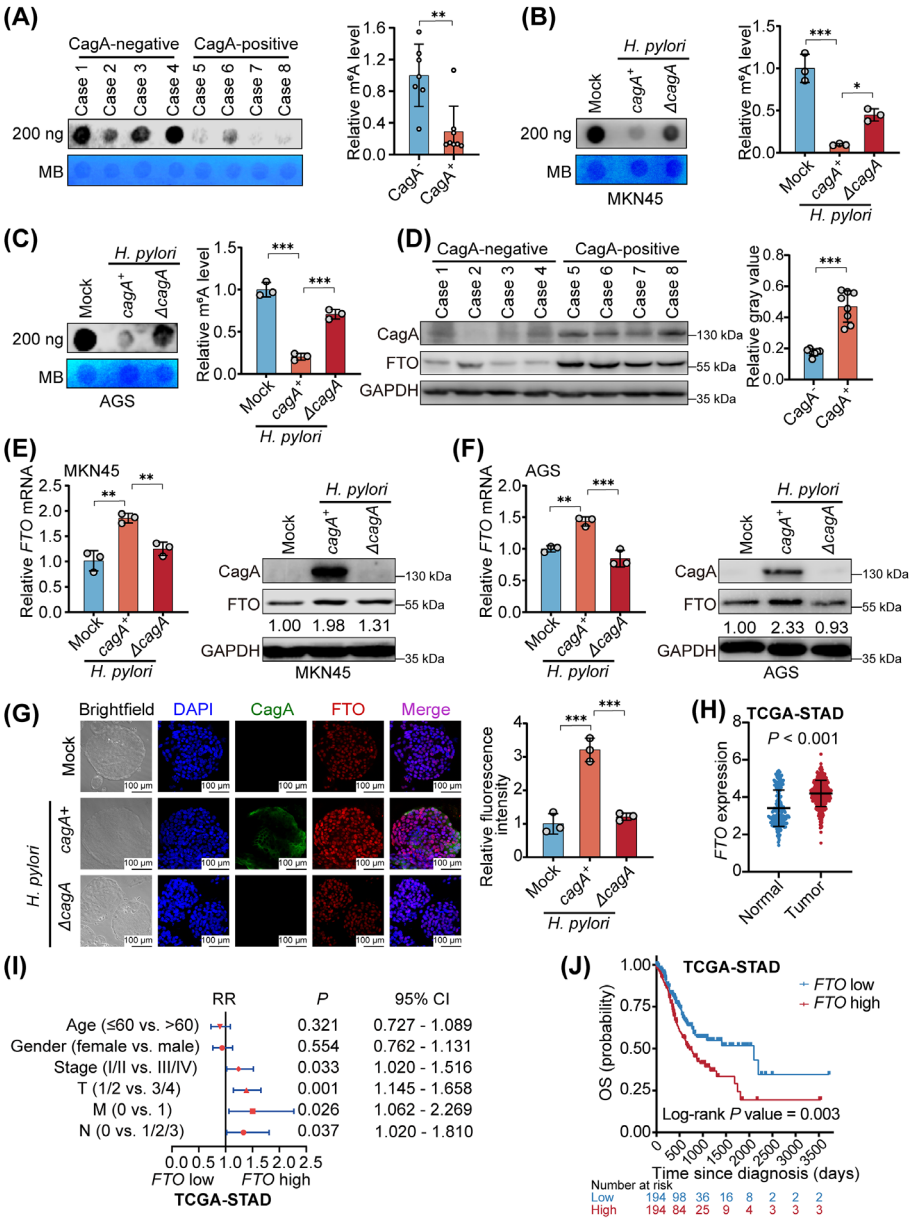

FIGURE 1 *cagA*$^+$ *H. pylori* mediates m^{6}A modification and induces *FTO* expression. (A) Representative image of dot-blotting assay to measure total m^{6}A levels in mRNA of GC tissues. The RNA sample loading amount was 200 ng. MB was used as a control. The relative quantification result is shown on the right. Data represented as mean ± SD. CagA$^+$, $n = 8$; CagA$^-$, $n = 7$. (B-C) Dot-blotting assay to measure total m^{6}A levels in mRNA of MKN45 (B) and AGS (C) cells after infection with *cagA*$^+$ or *ΔcagA H. pylori* for 24 hours. Mock, uninfected group, $n = 3$. (D) Representative image of western blotting results showed protein levels of FTO and CagA in GC samples. Quantification of the band intensities is shown on the right. (E-F) qRT-PCR and western blotting analysis on both mRNA and protein levels of FTO in MKN45 (E) and AGS (F) cells after *cagA*$^+$ or *ΔcagA H. pylori* infection. Mock, uninfected group, $n = 3$ for qRT-PCR. The numbers below the bands in the western blotting results represented the relative gray values of FTO quantification. (G) Representative images of immunofluorescence staining of DAPI, CagA and FTO in human GC organoids of the indicated group. Quantification of the fluorescence intensity was shown on the right. Scale bar, 100 μm. $n = 3$. (H) qRT-PCR result of *FTO* mRNA levels in GC ($n = 408$) tumor and normal tissues ($n = 211$) from the TCGA-STAD cohort. (I) Correlation analysis of *FTO* expression with clinicopathological features of GC patients in the TCGA-STAD cohort ($n = 408$). (J) Log-rank test indicating the OS of individuals with high or low *FTO* expression in the TCGA-STAD cohort. Samples were stratified into high and low expression groups based on the median expression levels of *FTO*. $^*P < 0.05$, $^{**}P < 0.01$, and $^{***}P < 0.001$ according to the unpaired *t*-test (A, D and H), one-way ANOVA (B, C, E, F and G), Pearson chi-square test (I) and log-rank test (J). Abbreviations: CagA, cytotoxin-associated gene A; CagA$^-$, CagA-negative; CagA$^+$, CagA-positive; *cagA*$^+$ *H. pylori*, *H. pylori cagA*$^+$ strain; CI, confidence interval; DAPI, 4',6-diamidine-2-phenylindole; FTO, fat mass and obesity-associated protein; GAPDH, glyceraldehyde 3-phosphate dehydrogenase; GC, gastric cancer; M, metastasis; m^{6}A, N^6-methyladenosine; MB, methylene blue stain; N, node; OS, overall survival; qRT-PCR, quantitative real-time PCR; RR, risk ratio; SD, standard deviation; STAD, stomach adenocarcinoma; T, tumor; TCGA, the Cancer Genome Atlas; *ΔcagA H. pylori*, *H. pylori* isogenic mutant strain.

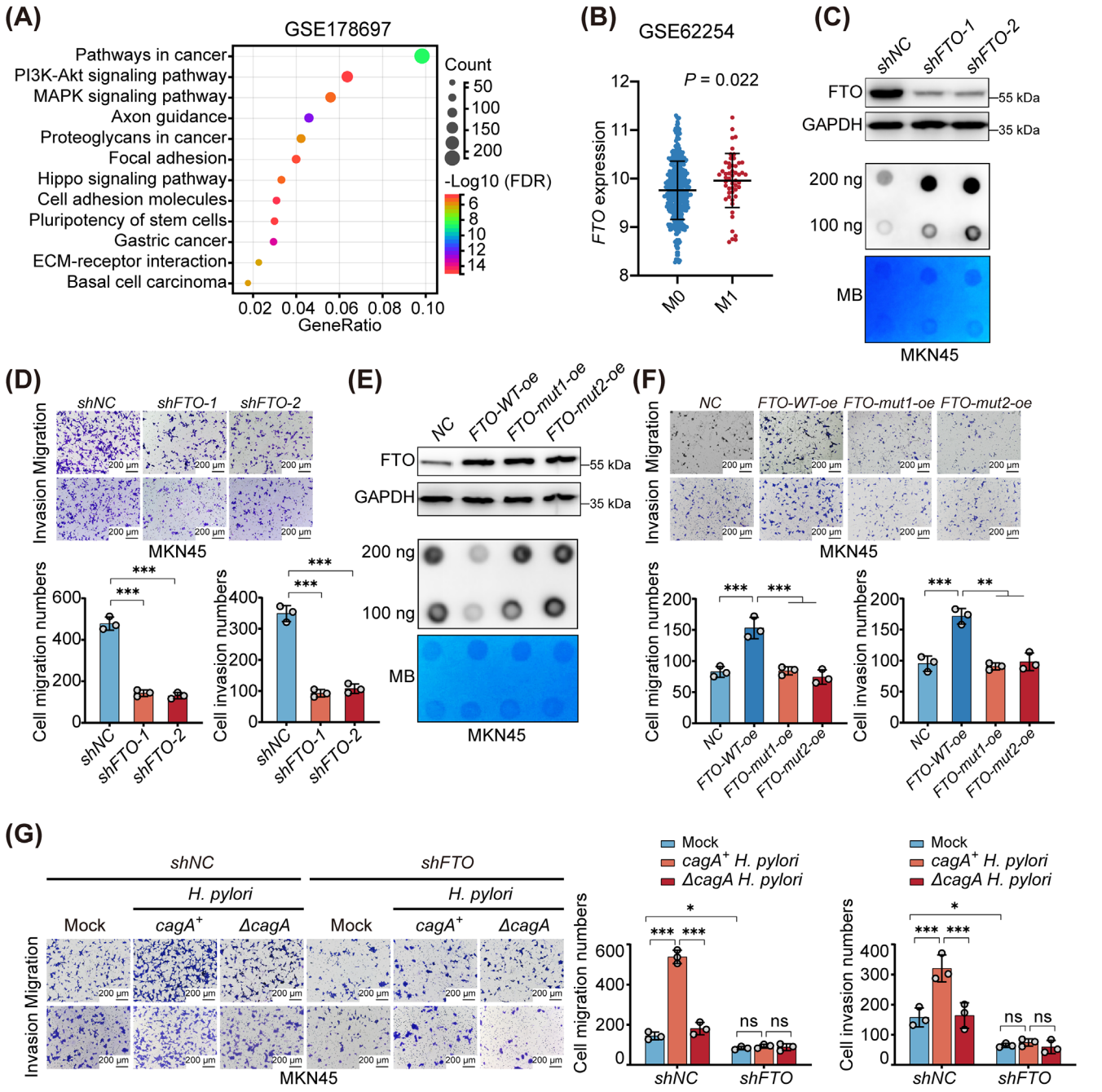

FIGURE 2 FTO is needed for CagA-induced GC metastasis. (A) KEGG enrichment analysis of gene altered in response to *FTO* knockdown in the GSE178697 dataset. (B) mRNA level of *FTO* in M0 ($n = 248$) and M1 ($n = 52$) group of GC tissues from the GSE62254 dataset. Data represented as mean ± SD. (C) Western blotting and dot-blotting assay to validate the *FTO* knockdown efficiency in MKN45 cells. The RNA sample loading amounts were 200 ng and 100 ng. MB was used as a control. (D) Representative image of migration and invasion assay with or without *FTO* knockdown in MKN45 cells. Quantification results are shown below. $n = 3$. Scale bar, 200 μm. (E) Western blotting and dot-blotting assay to validate overexpression of FTO in the *FTO-WT-oe*, *FTO-mut1-oe, and FTO-mut2-oe* groups in MKN45 cell. The RNA sample loading amounts were 200 ng and 100 ng. MB was used as a control in dot-blotting assay. (F) Representative images of migration and invasion assay of overexpressing *FTO-WT*, *FTO-mut1* or *FTO-mut2* in MKN45 cells. Quantification results were shown below. $n = 3$. Scale bar, 200 μm. (G) Representative images of migration and invasion assay of *FTO* knockdown in *cagA*$^+$ and *ΔcagA H. pylori*-infected MKN45 cells (left). Quantification results were shown on the right, $n = 3$. Scale bar, 200 μm. ns, not significant, $^*P < 0.05$, $^{**}P < 0.01$, $^{***}P < 0.001$ and $^{****}P < 0.0001$ according to unpaired *t*- tests (B and D) and one-way ANOVA (F and G). Abbreviations: *cagA*$^+$ *H. pylori*, *H. pylori cagA*$^+$ strain; FDR, false discovery rate; FTO, fat mass and obesity-associated protein; *FTO-mut*, mutant *FTO*; GAPDH, Glyceraldehyde 3-phosphate dehydrogenase; M0, no distant metastasis; M1, distant metastasis; MB, methylene blue stain; NC, negative control; SD, standard deviation; *shFTO*, short hairpin RNA against *FTO*; *shNC*, short hairpin RNA negative control; *ΔcagA H. pylori*, *H. pylori* isogenic mutant strain.

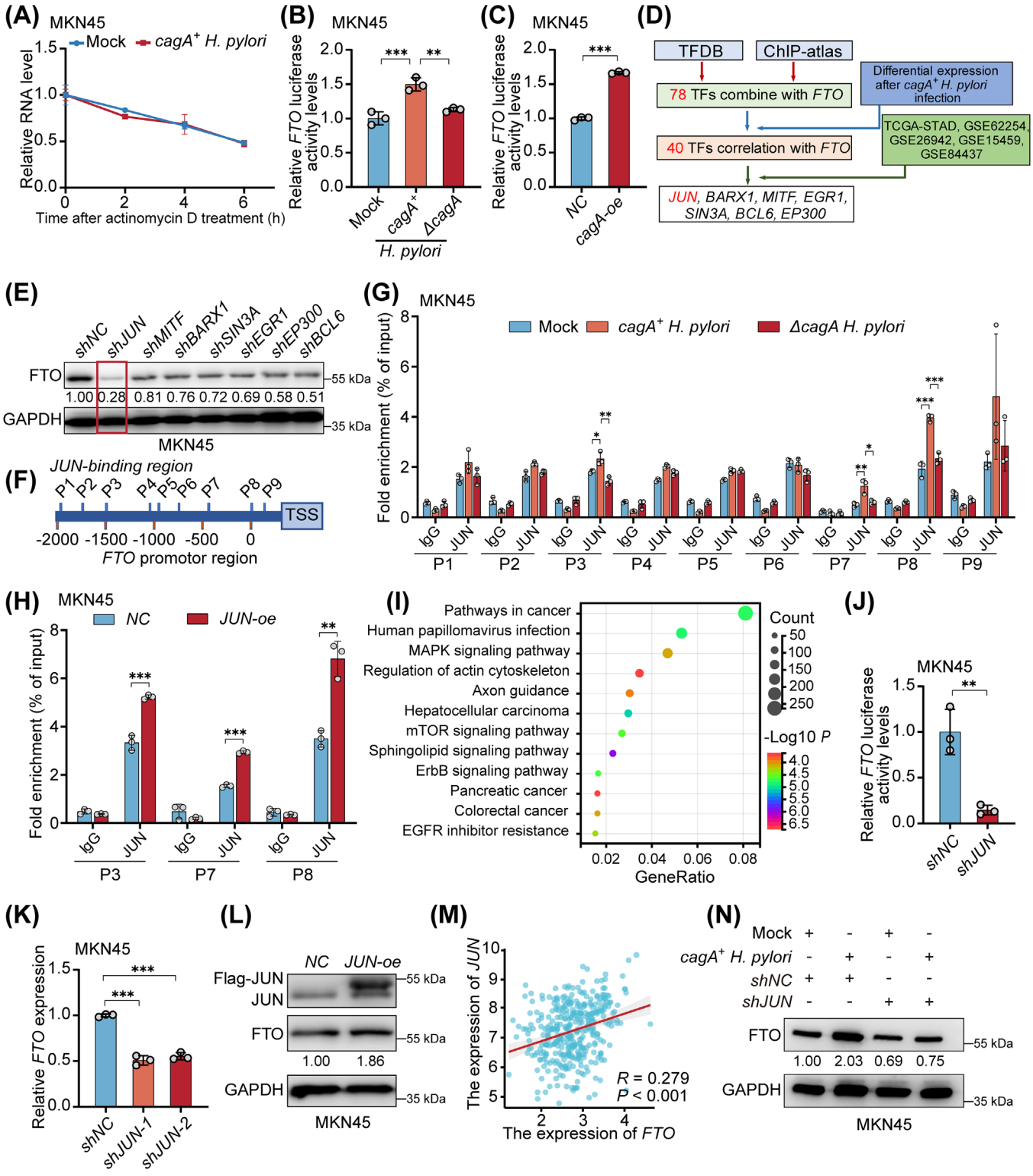

FIGURE 3 CagA promotes the binding of JUN to the promoter region of FTO to facilitate the expression of *FTO*. (A) mRNA stability of *FTO* after *cagA*$^+$ *H. pylori* infection in MKN45 cell. (B) Luciferase assay to measure *FTO* promoter activity in Mock, *ΔcagA H. pylori* infection, and *cagA*$^+$ *H. pylori* infection group of MKN45 cell. (C) Luciferase assay to measure *FTO* promoter activity in MKN45 cells with either NC or *cagA* overexpression. (D) Workflow for screening possible candidate TFs which can target *FTO* promoter. (E) Western blotting showed the protein level of FTO with the knockdown of seven candidate TFs in MKN45 cells. The numbers below the bands represented the relative gray values of FTO quantification. (F) Schematic showing the location of the predicted *JUN*-binding region in the *FTO* promoter. (G-H) ChIP assay showed enrichment of DNA fragments in the binding region within *cagA*$^+$ or *ΔcagA H. pylori*-infected (G) or *JUN*-overexpressed (H) MKN45 cells. (I) KEGG analysis of gene altered in response to *cagA*$^+$ *H. pylori* infection in MKN45 cells. (J) Luciferase assay to measure *FTO*

enhanced *FTO* promoter activity (Figure 3B-C). This prompted us to utilize the Animal TFDB and ChIP-atlas databases to identify the TFs that may interact with the *FTO* promoter region. Through further analysis of the correlation between the expression of these candidate TFs and *FTO* in our RNA-seq data from GC cells post-*cagA*$^+$ *H. pylori* infection, along with GC datasets from GEO and TCGA-STAD, we identified seven TFs as potential regulators of *FTO* expression (Figure 3D). Notably, among these, knockdown of *JUN* resulted in a significantly reduced expression of *FTO* (Figure 3E, Supplementary Figure S3A). We proceeded to investigate nine putative *JUN* binding sites within the *FTO* promoter, identified through JASPAR and Animal TFDB, and designed specific primers for validation (P1-P9) (Figure 3F). ChIP-PCR confirmed that the P3, P7, and P8 fragments were significantly enriched upon *cagA*$^+$ *H. pylori* infection (Figure 3G) and *JUN* overexpression (Figure 3H), indicating these regions as JUN-specific binding sites in the *FTO* promoter.

cagA$^+$ *H. pylori* infection upregulates *JUN* expression via MAPK, and the use of MAPK1/3 inhibitors attenuated the nuclear translocation of JUN [33]. Interestingly, genes with altered expression following *cagA*$^+$ *H. pylori* infection, as identified from our RNA-Seq data, were found to be significantly enriched in the mitogen-activated protein kinase (MAPK) pathway (Figure 3I). Kaplan-Meier analysis of the GSE62254 dataset revealed a significant positive relationship between elevated *JUN* levels and poor OS in GC patients (Supplementary Figure S3B). We further confirmed that *cagA*$^+$ *H. pylori* infection promotes *JUN* expression (Supplementary Figure S3C). *JUN* knockdown resulted in decreased *FTO* promoter activity (Figure 3J) and reduced mRNA level of *FTO* (Figure 3K, Supplementary Figure S3D), while overexpression of *JUN* promoted *FTO* expression (Figure 3L). Additionally, a positive correlation was observed between *FTO* and *JUN* expression levels (Figure 3M, Supplementary Figure S3E-G). The increase in *FTO* expression induced by *cagA*$^+$ *H. pylori* infection was abolished by *JUN* knockdown (Figure 3N, Supplementary Figure S3H). Consistent with these findings, *JUN* knockdown also eliminated the metastatic and invasive capabilities of GC cells induced by *cagA*$^+$ *H. pylori* infection (Supplementary Figure S3I-J). Collectively, our findings confirm that *cagA*$^+$ *H. pylori* infection promotes *FTO* transcription by activating JUN in GC cells.

3.4 | CagA-induced FTO elevation further promoted EMT in GC cells

To identify candidate targets of the CagA-FTO axis, MeRIP-seq and RNA-seq were conducted on MKN45 cells with or without *cagA*$^+$ *H. pylori* infection (Supplementary Figure S4A). MeRIP-Seq results indicated that mRNAs from the *cagA*$^+$ *H. pylori*-infected group exhibited a lower number of m^{6}A peaks compared to the non-infected control group. (Supplementary Figure S4B). Notably, a total of 1,622 genes with m^{6}A altered peaks exhibited downregulation, while 2,151 genes showed upregulation in expression after *cagA*$^+$ *H. pylori* infection (Supplementary Figure S4C). GO analysis indicated that genes with altered m^{6}A peaks and differential expression after *cagA*$^+$ *H. pylori* infection were substantially enriched in processes related to cell polarity, including cytoskeleton and microtubule organization (Supplementary Figure S4D). By intersecting data from our RNA-seq and MeRIP-seq with RNA-seq data from the GSE178697, we identified 336 genes that displayed decreased m^{6}A modification and altered expression following *FTO* knockdown and *H. pylori* infection (Supplementary Figure S4E), suggesting their potential as downstream targets of the CagA-FTO axis. These candidate targets were notably enriched in the EMT pathway, as assessed via GSVA (Supplementary Figure S4F). The microsatellite stable/epithelial-to-mesenchymal transition (MSS/EMT) subtype of GC, known for its aggressive nature and unfavorable prognosis [34], showed significantly elevated *FTO* expression levels compared to other subtypes in our analysis of the GSE62254 dataset (Supplementary Figure S4G). The EMT score, based on the expression differences of known epithelial and mesenchymal markers

promoter activity when *JUN* was knockdown in MKN45 cells. (K) qRT-PCR analysis of *FTO* mRNA level after knockdown of *JUN* in MKN45 cells. (L) Western blotting showed protein levels of FTO with or without *JUN* overexpression in MKN45 cells. The numbers below the bands represented the relative gray values of FTO quantification. (M) Correlation between *FTO* and *JUN* expression in GC tissues from the TCGA-STAD cohort ($n = 408$). (N) Western blotting to detect the expression level of FTO with *JUN* knockdown and exposure to *cagA*$^+$ *H. pylori* in MKN45 cells. The numbers below the bands represented the relative gray values of FTO quantification. $^*P < 0.05$, $^{**}P < 0.01$, and $^{***}P < 0.001$ were determined through one-way ANOVA (B and G), unpaired *t*-tests (C, H, J and K) and Pearson correlation analysis (N). Abbreviations: BARX1, Basic region leucine zipper 1; BCL6, B-cell lymphoma 6; CHIP, chromatin immunoprecipitation; EGR1, Early growth response 1, SIN3A, SIN3 homolog A, histone deacetylase complex subunit; EP300, E1A binding protein p300; FTO, fat mass and obesity-associated protein; GAPDH, Glyceraldehyde 3-phosphate dehydrogenase; IgG, Immunoglobulin G; JUN, Jun Proto-Oncogene; MITF, Microphthalmia-associated transcription factor; P1-P9, JUN binding sites within the *FTO* promoter; TFDB, the Animal Transcription Factor DataBase; TFs, transcription factors; TSS, transcription start site.

[35], showed a positive correlation with *FTO* expression in GC tissues from the TCGA-STAD cohort (Supplementary Figure S4H). GSEA further confirmed that the EMT molecular signature was notably enriched in GC samples with high *FTO* expression compared to those with low *FTO* expression (Supplementary Figure S4I).

The expression of mesenchymal markers, including N-cadherin, Snail, and Vimentin, was substantially reduced in the *FTO* knockdown group compared to the control group, while E-cadherin expression was increased (Supplementary Figure S4J). Conversely, overexpression of *FTO*, but not its mutant forms, significantly elevated the expression of mesenchymal markers (Supplementary Figure S4K). Moreover, *FTO* knockdown in GC cells reversed the EMT process induced by *cagA*$^+$ *H. pylori* infection (Supplementary Figure S4L). Overall, these findings suggest that elevated *FTO* expression following *cagA*$^+$ *H. pylori* infection may activate EMT, which may account for the pro-oncogenic effects of the bacterial infection.

3.5 | HBEGF served as the primary downstream target of the CagA-FTO axis

To deepen our comprehension of the CagA-FTO axis's regulatory role in EMT, we intersected the 336 putative downstream targets with the EMT-associated genes from the EMTome database (Figure 4A). *HBEGF*, *FKBP5*, *EPB41L3*, *EPHA8*, *PGF*, *KRT18*, *MAGED1*, *PHLDA2*, *WNT3A*, *and TIAM1* were determined to be regulated by FTO. Further analysis identified *HBEGF* as the gene exhibiting the most striking reduction in response to *FTO* knockdown (Supplementary Figure S5A). In addition, HBEGF expression was notably elevated in GC cells infected with *cagA*$^+$ *H. pylori* compared to those infected with *ΔcagA H. pylori* or uninfected (Figure 4B). Our Western blot analysis further confirmed that *FTO* knockdown reduced *HBEGF* expression in GC cells (Figure 4C). Conversely, only *FTO-WT-oe*, rather than mutant forms *FTO-mut1-oe* and *FTO-mut2-oe*, substantially increased *HBEGF* expression (Figure 4D). Furthermore, the elevation of *HBEGF* induced by *cagA*$^+$ *H. pylori* was reversed by *FTO* knockdown (Figure 4E), establishing HBEGF as a primary downstream target of the CagA-FTO axis. A positive correlation was observed between *HBEGF* levels and the EMT score in the vast majority of tumor types (Supplementary Figure S5B). GC patients with elevated *HBEGF* expression also showed poor OS (Supplementary Figure S5C). Studies have implicated secreted HBEGF in promoting EMT [36–38]. We confirmed that *cagA*$^+$ *H. pylori* infection and *FTO* overexpression significantly increased HBEGF secretion, while *FTO* knockdown reduced HBEGF secretion (Figure 4F-H).

HBEGF knockdown markedly reduced GC cell metastasis and invasion (Supplementary Figure S5D-E) and negated the pro-EMT and pro-metastatic effects induced by *cagA*$^+$ *H. pylori* infection (Figure 4I, Supplementary Figure S5F-G). To further uncover the m^{6}A modification sites on *HBEGF* mRNA regulated by FTO, we utilized the SRAMP database to predict four m^{6}A modification sites on *HBEGF* mRNA with "very high confidence" (Supplementary Figure S6A). On the basis of these four sites, we designed specific primers and further confirmed them via MeRIP-qPCR. Results showed that *FTO* knockdown significantly elevated the level of m^{6}A modification at sites 418, 448, and 1304 in MKN45 cells (Figure 4J), and at sites 418 and 448 in AGS cells (Supplementary Figure S6B). Consequently, we infer that sites 418 and 448 may be the m^{6}A sites specifically targeted by FTO on *HBEGF* mRNA. Moreover, the m^{6}A modifications at these sites were markedly reduced by the overexpression of *FTO-WT*, compared with NC and *FTO-mut1*/*FTO-mut2* (Figure 4K, Supplementary Figure S6C). Taken together, these findings indicated that FTO can specifically target m^{6}A sites on *HBEGF* mRNA, modulating its m^{6}A modification level.

3.6 | FTO increased the stability of *HBEGF* mRNA via YTHDF2

m^{6}A readers have been reported to control the stability, translation, and shearing of RNA [25, 39]. To identify m^{6}A readers that target *HBEGF* mRNA, we performed mass spectrometry analysis following an RNA pull-down assay (Supplementary Tables S7-S8). Among three replicates, 135 candidate proteins were screened out. After exhaustive research in specialized databases and literature, only YTHDF2 was reported as an m^{6}A "reader" among these proteins [25]. Thus, we suggest that YTHDF2 may be a candidate for binding to *HBEGF* mRNA (Figure 5A). RIP and RNA pull-down assays confirmed that YTHDF2 binds to *HBEGF* mRNA (Figure 5B-C). YTHDF2, a protein known to target m^{6}A sites and decrease mRNA stability [25], exhibited a significant elevation in *HBEGF* expression following *YTHDF2* knockdown, as compared to the control group (Figure 5D, Supplementary Figure S7A). Furthermore, *YTHDF2* knockdown significantly enhanced *HBEGF* mRNA stability (Figure 5E), whereas *FTO* knockdown reduced it (Figure 5F). In addition, only the overexpression in cells with *FTO-WT-oe*, but not with *FTO-mut1-oe* and *FTO-mut2-oe*, was found to increase *HBEGF* mRNA stability (Figure 5G, Supplementary Figure S7B).

An inverse relationship was identified between the expression levels of *YTHDF2* and those of *HBEGF* and *FTO* (Figure 5H, Supplementary Figure S7C-E). Furthermore,

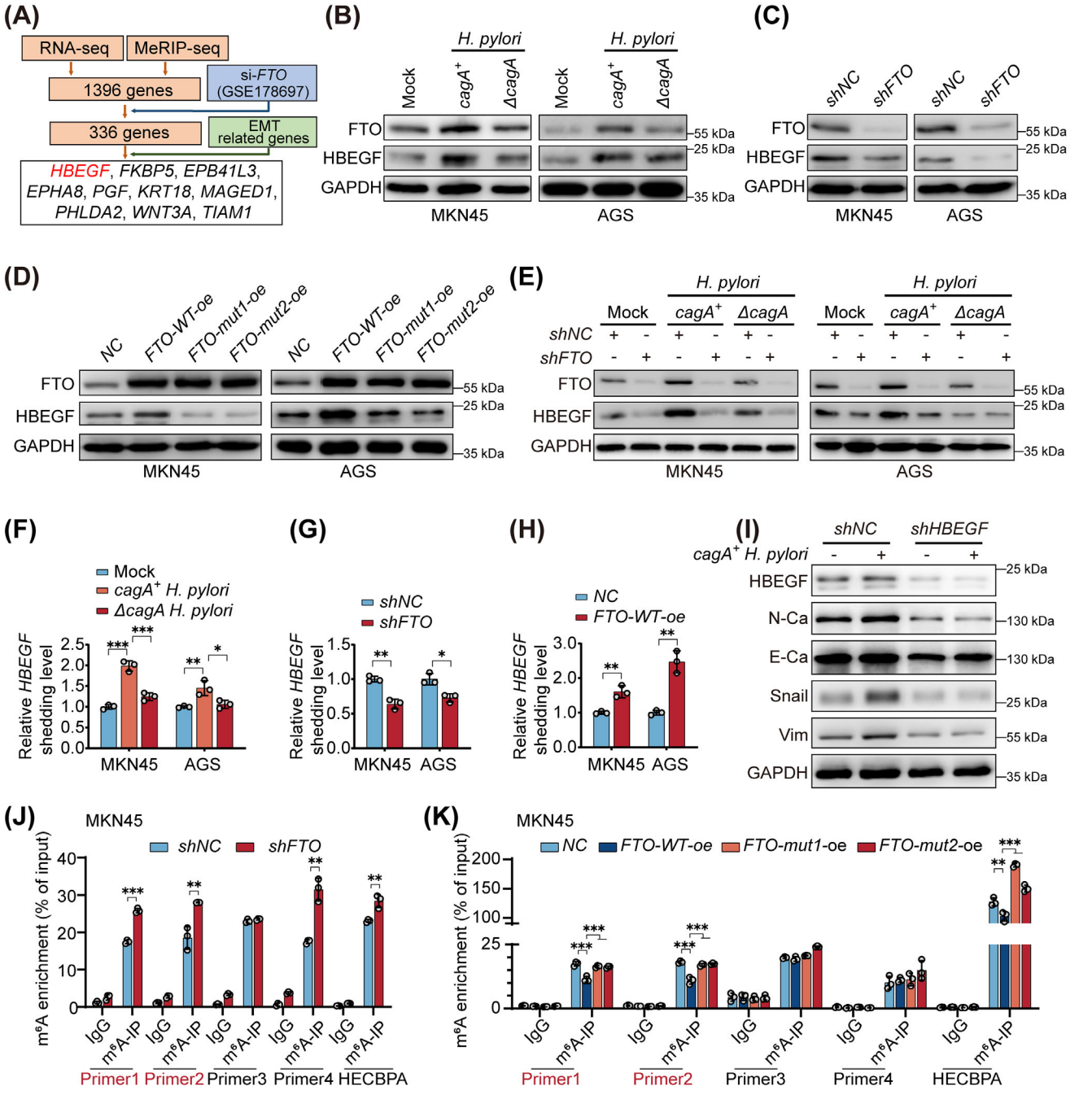

FIGURE 4 HBEGF serves as the primary downstream target of the CagA-FTO axis. (A) Workflow showed the screening strategy for candidate targets of the CagA-FTO axis. (B) Western blotting to detect the protein level of FTO and HBEGF in GC cells after exposed to *cagA*$^+$ or *ΔcagA H. pylori*. (C) Western blotting to detect the protein level of FTO and HBEGF in GC cells with or without *FTO* knockdown. (D) Western blotting is used to detect the protein levels of FTO and HBEGF in GC cells overexpressing wild-type *FTO-WT*, *FTO-mut1*, or *FTO-mut2*. (E) Western blotting showed protein levels of FTO and HBEGF in NC and *FTO* knockdown GC cells exposed to *cagA*$^+$ or *ΔcagA H. pylori*. (F-H) ELISA assay showed secretion level of *HBEGF* in the culture supernatants of *H. pylori*-infected (F), *FTO* knockdown (G) and *FTO* overexpressing (H) GC cells. (I) Western blotting to detect the expression levels of EMT markers in GC cells with *HBEGF* knockdown and *cagA*$^+$ *H. pylori* exposure. (J-K) MeRIP-qPCR showed enrichment of m^{6}A modification on *HBEGF* mRNA after *FTO* knockdown (J) and *FTO* overexpression (wild-type *FTO* or mutated *FTO*, K). HECBPA was used as a positive control. ns, not significant, $^*P < 0.05$, $^{**}P < 0.01$, and $^{***}P < 0.001$ were determined through one-way ANOVA (F and K) and unpaired *t*-tests (G, H and J). Abbreviations: E-Ca, E-cadherin; EMT, epithelial-mesenchymal transition; *FTO mut*, mutant *FTO*; FTO, fat mass and obesity-associated protein; GAPDH, Glyceraldehyde 3-phosphate dehydrogenase; MeRIP-seq, Methylated RNA immunoprecipitation sequencing; HBEGF, heparin-binding EGF like growth factor; HECBPA, 2'-O-methyladenosine-3'-phosphate-5'-phosphate; IgG, Immunoglobulin G; m^{6}A-IP, Methylated RNA immunoprecipitation; N-Ca, N-cadherin; Vim, Vimentin.

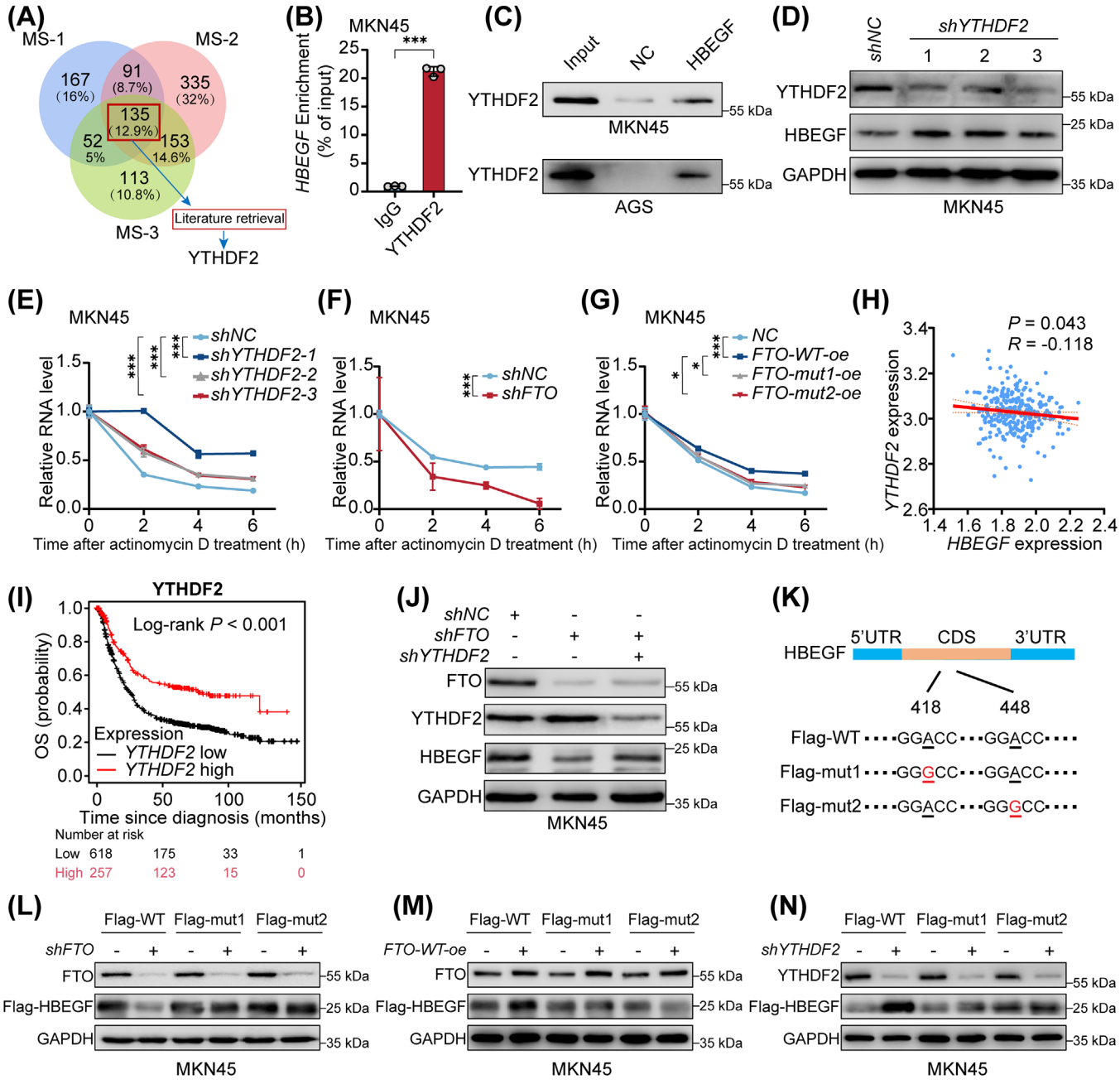

FIGURE 5 FTO increases the stability of *HBEGF* mRNA via YTHDF2. (A) Venn diagram showing 135 common genes among three times of repetition from MS results. (B) RIP-qPCR verified the enrichment of *HBEGF* mRNA on YTHDF2 protein in MKN45 cells. (C) RNA pull-down showing the binding of *HBEGF* mRNA to YTHDF2. (D) Western blotting showed an upregulated protein level of *HBEGF* with *YTHDF2* knockdown in MKN45 cells. (E-G) qRT-PCR analysis of *HBEGF* mRNA in the indicated group when MKN45 cells were exposed to actinomycin D, with or without *YTHDF2* knockdown (E), with or without *FTO* knockdown (F) and with or without *FTO* overexpression (G). (H) Expression correlation between *HBEGF* and *YTHDF2* levels in GC tissues from the TCGA-STAD cohort ($n = 408$). (I) Log-rank test indicating the OS of individuals with high ($n = 257$) or low ($n = 618$) *YTHDF2* expression in the GSE62254. (J) Western blotting showed protein level of *HBEGF* in MKN45 cells with *FTO* knockdown or *YTHDF2* knockdown. (K) Schematic showing the construction of Flag-tagged wild-type or m^6A modification site-mutant *HBEGF* probes. (L-N) Western blotting showed protein level of Flag-tagged *HBEGF* in MKN45 cells among indicated groups, with or without *FTO* knockdown (L), with or without *FTO* overexpression (M) and with or without *YTHDF2* knockdown (N). $^{*}P < 0.05$ and $^{***}P < 0.001$ according to the unpaired *t*-test (B), two-way ANOVA (E to G), Pearson correlation tests (H) and log-rank test (I). Abbreviations: 3'UTR, 3'untranslation region; 5'UTR, 5'untranslation region; CDS, Coding DNA Sequence; Flag-mut, Flag-labeled mutant *HBEGF*; Flag-WT, Flag-labeled wild-type *HBEGF*; *FTO mut*, mutant *FTO*; *FTO*, fat mass and obesity-associated protein; GAPDH, Glyceraldehyde 3-phosphate dehydrogenase; *HBEGF*, heparin-binding EGF like growth factor; MS, mass spectrometry; *NC*, negative control; YTHDF2, YTH N(6)-methyladenosine RNA binding protein 2.

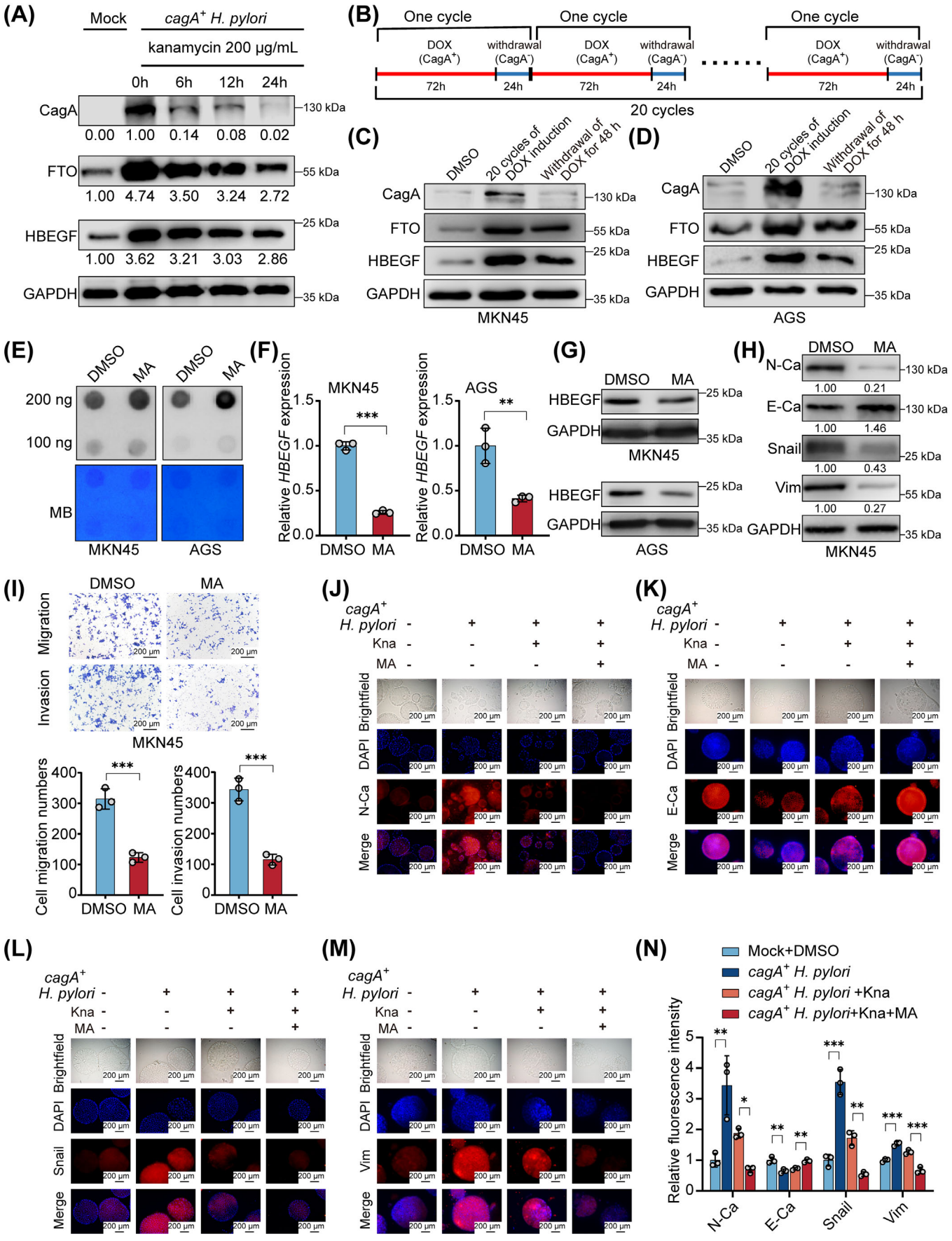
(A)
Mock
cagA+ H. pylori
kanamycin 200 μg/mL
0h 6h 12h 24h
CagA
0.00 1.00 0.14 0.08 0.02
130 kDa
FTO
1.00 4.74 3.50 3.24 2.72
55 kDa
HBEGF
1.00 3.62 3.21 3.03 2.86
25 kDa
GAPDH
35 kDa
(B)
One cycle
One cycle
One cycle
DOX (CagA+)
withdrawal (CagA-)
72h
24h
20 cycles
(C)
DMSO
20 cycles of DOX induction
Withdrawal of DOX for 48 h
MKN45
(D)
AGS
(E)
200 ng
100 ng
MB
MKN45
AGS
(F)
Relative HBEGF expression
MKN45
AGS
***
**
DMSO MA
(G)
HBEGF
GAPDH
(H)
N-Ca
E-Ca
Snail
Vim
1.00 0.21
1.00 1.46
1.00 0.43
1.00 0.27
(I)
Migration
Invasion
200 μm
Cell migration numbers
Cell invasion numbers
(J)
cagA+ H. pylori
Kna
MA
Brightfield
DAPI
N-Ca
Merge
(K)
E-Ca
(L)
Snail
(M)
Vim
(N)
Mock+DMSO
cagA+ H. pylori
cagA+ H. pylori +Kna
cagA+ H. pylori+Kna+MA
Relative fluorescence intensity
N-Ca
E-Ca
Snail
Vim

elevated *YTHDF2* expression in GC tissue was associated with better patient outcomes (Figure 5I). *YTHDF2* knockdown in GC cells with stable *FTO* knockdown rescued *HBEGF* expression (Figure 5J, Supplementary Figure S7F). To ascertain whether FTO and YTHDF2 modulate *HBEGF* expression through m^{6}A modification, we stably expressed wild-type *HBEGF* with a Flag tag and *HBEGF* mutations at the 418 or 448 m^{6}A sites (Figure 5K, Supplementary Figure S7G), as previously validated (Figure 4J-K). Neither FTO nor YTHDF2 influenced *HBEGF* expression after mutation of the m^{6}A sites in HBEGF (Figure 5L-N, Supplementary Figure S7H-I). These results indicate that YTHDF2 exploits the 418 and 448 m^{6}A sites to regulate *HBEGF* mRNA stability.

3.7 | MA treatment impeded the progression of GC following *H. pylori* eradication

The "hit-and-run" hypothesis posits that *H. pylori* eradication may not prevent the progression of GC [18, 19]. In line with this hypothesis, we observed that although CagA was substantially eliminated in GC cells following antibiotic treatment, the levels of *FTO* and *HBEGF* did not revert to baseline but remained elevated compared to the uninfected group (Figure 6A, Supplementary Figure S8A). To explore this phenomenon, we constructed a DOX-CagA-tet-on system, which allows DOX-inducible overexpression of *cagA*, as previously described [18]. Mimicking chronic *cagA*$^+$ *H. pylori* infection with intermittent delivery of CagA via T4SS, we induced CagA by 20 cycles of DOX (Figure 6B). This repeated induction of CagA promoted *FTO* and *HBEGF* expression, and even after 48 hours of cessation of CagA induction, their expression levels remained elevated (Figure 6C-D, Supplementary Figure S8B), suggesting that repeated exposure with *cagA*$^+$ *H. pylori* could induce irreversible epigenetic alterations.

MA, a nonsteroidal anti-inflammatory drug (NSAID) approved by the U.S. Food and Drug Administration (FDA) [40], has been reported to selectively inhibit the m^{6}A demethylation activity of FTO without affecting AlkB homolog 5 (*ALKBH5*) [41]. Treatment with MA increased the m^{6}A level (Figure 6E) and significantly suppressed *HBEGF* expression (Figure 6F-G), as well as the levels of N-cadherin, Vimentin and Snail, while upregulating E-Ca (Figure 6H). Consistently, MA disrupted the migration and invasion capabilities of GC cells (Figure 6I, Supplementary Figure S8C). These effects were also verified in human GC organoids, where MA treatment inhibited the EMT process (Supplementary Figure S8D-G). To assess the combined therapeutic effect of MA and antibiotics on GC, organoids were treated with MA and kanamycin following infection with *cagA*$^+$ *H. pylori*. Eradication of *H. pylori* post-infection mitigated the EMT process, characterized by increased E-cadherin and decreased N-cadherin, Snail, and Vimentin; importantly, subsequent MA treatment further inhibited EMT activation (Figure 6J-N). Collectively, these findings indicate that *cagA*$^+$ *H. pylori* infection may induce irreversible alterations in the oncogenic pathway through m^{6}A modification, and MA therapy potentially blocks CagA-induced EMT and the metastatic capacity of GC cells.

3.8 | CagA targeted FTO to promote GC metastasis in vivo

We extended our investigation to in vivo models to assess the impact of FTO on GC metastasis. A mouse model of tumor metastasis was established by tail vein inoculation of GC cells. Notably, *FTO* knockdown significantly

FIGURE 6 MA treatment impeded the progression of GC following *H. pylori* eradication. (A) Western blotting showed protein levels of FTO and HBEGF after *cagA*$^+$ *H. pylori* infection and kanamycin therapy in MKN45 cells. The numbers below the bands represented the relative gray values of quantification. (B) Schematic showing construction of the CagA-tet-on system for the cycling CagA induction process. (C-D) Western blotting showed protein levels of *FTO* and *HBEGF* in MKN45 (C) and AGS (D) cells after 20 cycles of CagA induction and withdrawal of DOX for 48 hours. (E) Dot-blotting assay showed m^{6}A levels in MKN45 (left) and AGS (right) cells treated with MA or DMSO. (F-G) qRT-PCR (F) and western blotting (G) showed the expression level of *HBEGF* when GC cells were treated with MA or DMSO. (H) Western blotting showed protein levels of EMT markers in response to MA treatment. The numbers below the bands represented the relative gray values of quantification. (I) Migration and invasion assay showed the suppressive effect of MA on MKN45 cells. Quantification results are shown below. $n = 3$. Scale bar, 200 μm. (J-M) Representative image of immunofluorescence staining in GC organoids exposed to indicated groups, N-ca (J), E-ca (K), Snail (L) and Vim (M). Scale bar, 200 μm. (N) Quantification results of fluorescence intensity among EMT markers using ImageJ software. $^*P < 0.05$, $^{**}P < 0.01$, and $^{***}P < 0.001$ according to unpaired *t*-tests (F and I) and one-way ANOVA (N). Abbreviations: CagA$^-$, CagA uninduced; CagA$^+$, CagA induced; DAPI, 4',6-diamidine-2-phenylindole; DMSO, Dimethyl sulfoxide; DOX, doxycycline; E-Ca, E-cadherin; EMT, epithelial-mesenchymal transition; FTO, fat mass and obesity-associated protein; GAPDH, Glyceraldehyde 3-phosphate dehydrogenase; HBEGF, heparin-binding EGF like growth factor; Kna, kanamycin; MA, meclofenamic acid; MB, Methylene blue stain; N-Ca, N-cadherin; Vim, Vimentin.

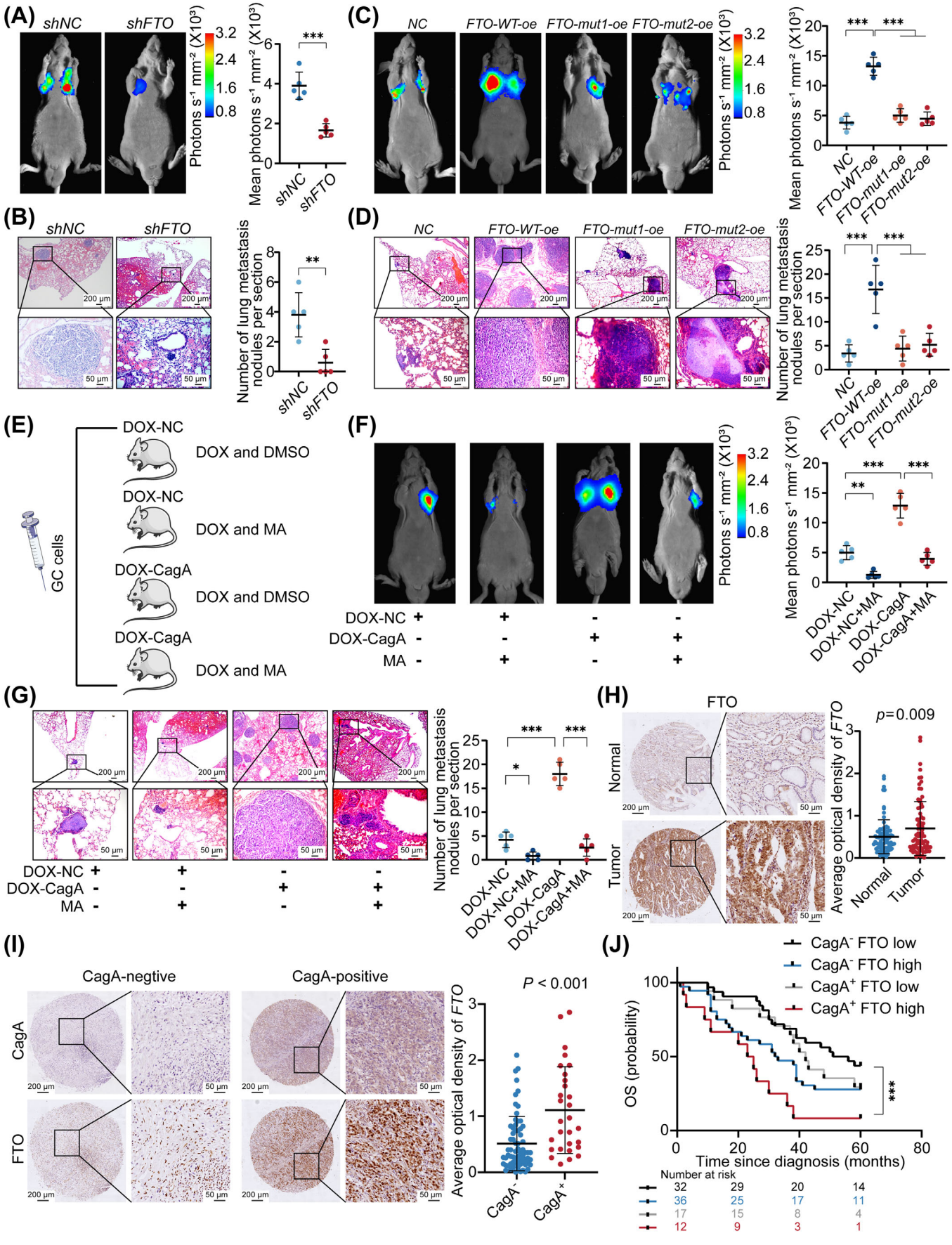
(A)
shNC
shFTO
Photons s⁻¹ mm⁻² (X10³)
3.2
2.4
1.6
0.8
Mean photons s⁻¹ mm⁻² (X10³)
***
shNC
shFTO
(B)
shNC
shFTO
200 μm
50 μm
Number of lung metastasis nodules per section
**
shNC
shFTO
(C)
NC
FTO-WT-oe
FTO-mut1-oe
FTO-mut2-oe
Photons s⁻¹ mm⁻² (X10³)
3.2
2.4
1.6
0.8
Mean photons s⁻¹ mm⁻² (X10³)
***
***
NC
FTO-WT-oe
FTO-mut1-oe
FTO-mut2-oe
(D)
NC
FTO-WT-oe
FTO-mut1-oe
FTO-mut2-oe
200 μm
50 μm
Number of lung metastasis nodules per section
***
***
NC
FTO-WT-oe
FTO-mut1-oe
FTO-mut2-oe
(E)
GC cells
DOX-NC
DOX and DMSO
DOX-NC
DOX and MA
DOX-CagA
DOX and DMSO
DOX-CagA
DOX and MA
(F)
Photons s⁻¹ mm⁻² (X10³)
3.2
2.4
1.6
0.8
DOX-NC + + - -
DOX-CagA - - + +
MA - + - +
Mean photons s⁻¹ mm⁻² (X10³)
**
***
***
DOX-NC
DOX-NC+MA
DOX-CagA
DOX-CagA+MA
(G)
200 μm
50 μm
DOX-NC + + - -
DOX-CagA - - + +
MA - + - +
Number of lung metastasis nodules per section
*
***
***
DOX-NC
DOX-NC+MA
DOX-CagA
DOX-CagA+MA
(H)
FTO
Normal
Tumor
200 μm
50 μm
p=0.009
Average optical density of FTO
Normal
Tumor
(I)
CagA-negtive
CagA-positive
CagA
FTO
200 μm
50 μm
P < 0.001
Average optical density of FTO
CagA⁻
CagA⁺
(J)
CagA⁻ FTO low
CagA⁻ FTO high
CagA⁺ FTO low
CagA⁺ FTO high
OS (probability)
***
Time since diagnosis (months)
Number at risk
32 29 20 14
36 25 17 11
17 15 8 4
12 9 3 1

inhibited lung metastasis of GC cells (Figure 7A-B, Supplementary Figure S8H). Conversely, overexpression of *FTO-WT*, but not *FTO-mut1* and *FTO-mut2*, led to an increase in the number of lung metastases (Figure 7C-D). To explore the therapeutic potential of MA in reversing CagA-promoted GC metastasis in vivo, CagA-tet-on cells were inoculated via the tail vein, followed by treatment with DOX and MA for 30 days (Figure 7E). The results showed that DOX-induced CagA significantly promoted the lung metastasis of GC cells. However, MA treatment effectively abolished the contribution of CagA on cell metastasis in the lungs (Figure 7F-G).

To further validate the above results in GC patients, expression of *cagA* and *FTO* were analyzed in two TMAs of GC samples. *FTO* expression was found to be noticeably elevated in GC tissues (Figure 7H). Importantly, *FTO* levels were considerably higher in CagA-positive GC tissues compared with CagA-negative GC tissues (Figure 7I). Moreover, the presence of CagA and increased *FTO* expression in GC patients were correlated with poor outcomes (Figure 7J). Collectively, the findings from both mouse models and clinical GC patients underscore the role of the CagA-FTO axis in driving GC progression.

4 | DISCUSSION

Although the interaction between *H. pylori* and the host has a significant impact on the development of GC, the underlying mechanisms remain largely unclear [42, 43]. Our research provided evidence that CagA delivery by *H. pylori* reduced total m^{6}A levels and promoted *FTO* expression in GC cells, which facilitated the metastatic potential of GC. We clearly demonstrated that CagA reduced m^{6}A modification in biomolecules linked to EMT, particularly *HBEGF*, by increasing *FTO* transcription through JUN. *HBEGF* expression was elevated as a consequence of the reduced m^{6}A modification, which prevented YTHDF2-dependent mRNA from degrading. Importantly, the results we gathered highlight MA's potential effectiveness as an FTO antagonist to prevent the progression of GC. MA administration was successful in preventing EMT in GC cells, and it showed efficacy in inhibiting GC metastasis in both animal models and human GC organoids. The results not only indicate that FTO inhibitors are potential drugs for GC treatment but also, more importantly, provide novel insights into the "hit-and-run" mechanism of CagA-induced GC development from an epigenetic perspective (Figure 8).

As the most abundant form of RNA modification, m^{6}A is dynamically altered in response to environmental and physiological influences and plays a crucial role in the development of multiple types of cancers [23, 44]. It is now established that several microbes have the capacity to modulate the m^{6}A landscape of their hosts [20], with these epigenetic alterations supporting microbial replication and influencing the host's disease process [45, 46]. Abnormal expression of FTO has been observed across multiple tumor types [47–49]. Additionally, FTO has been implicated in the malignant development of tumors caused by environmental alterations [21, 50]. Our results also demonstrated that CagA, a bacterial protein delivered by *H. pylori*, upregulated *FTO* expression and facilitated the EMT process. Both the results of previous studies and our research suggest that FTO is a responsive factor to environmental stress and plays a significant role in tumor progression.

The process of tumor metastasis, which involves a series of steps, initially stages with EMT [51, 52]. The activation

FIGURE 7 CagA promotes GC metastasis via FTO in vivo. (A) Bioluminescence imaging of the lung metastasis burden after inoculation of MKN45 cells with or without *FTO* knockdown (left). Quantification results were shown on the right, $n = 5$. (B) Representative images of HE staining of lung sections from the NC and *FTO* knockdown groups (left). The number of metastatic nodules was calculated (right). The scale bar was 200 μm (upper panels) or 50 μm (lower panels). $n = 5$. (C) Bioluminescence imaging of the lung metastasis burden after inoculation of MKN45 cells with *FTO-WT*, *FTO-mut1* or *FTO-mut2* overexpression (left). Quantification results were shown on the right. $n = 5$. (D) Representative images of HE staining of lung sections from the *FTO-WT*, *FTO-mut1*or *FTO-mut2* overexpressing groups. The scale bar was 200 μm (upper panels) or 50 μm (lower panels). $n = 5$. (E) Experimental design of the lung metastasis assay with MKN45 cells treated with DOX-induced CagA and MA. (F) Bioluminescence imaging of the lung metastasis burden after inoculation of MKN45 cells with DOX-induced CagA expression and MA treatment. Quantification results were shown on the right. $n = 5$. (G) Representative images of HE staining of lung sections from the indicated group. Quantification results about the number of lung metastases were shown on the right. The scale bar was 200 μm (upper panel) or 50 μm (lower panel). $n = 5$. (H) Representative images of FTO IHC staining in GC TMAs (left) and mean optical density statistics of FTO staining (right). The scale bar was 200 μm (left panel) or 50 μm (right panel). normal, $n = 83$; tumor, $n = 83$. (I) Representative IHC staining of FTO in CagA-positive and CagA-negative GC tissues from TMAs. The scale bar was 200 μm (left panel) or 50 μm (right panel). CagA-positive, $n = 29$; CagA-negative, $n = 68$. (J) Kaplan-Meier curves indicate the OS of individuals of the indicated groups in TMAs. $^{**}P < 0.01$ and $^{***}P < 0.001$ were determined through unpaired *t*-tests (A, B, H and I), one-way ANOVA (C, D, F and G), and log-rank tests (J). Abbreviations: CagA$^-$, CagA-negative; CagA$^+$, CagA-positive; DMSO, Dimethyl sulfoxide; DOX, doxycycline; DOX-CagA, DOX-induced *cagA* expression; FTO, fat mass and obesity-associated protein; *FTO-mut*, mutant *FTO*; GC, gastric cancer; HE, hematoxylin and eosin stain; IHC, immunohistochemical; MA, meclofenamic acid; NC, negative control; TMA, tissue microarray.

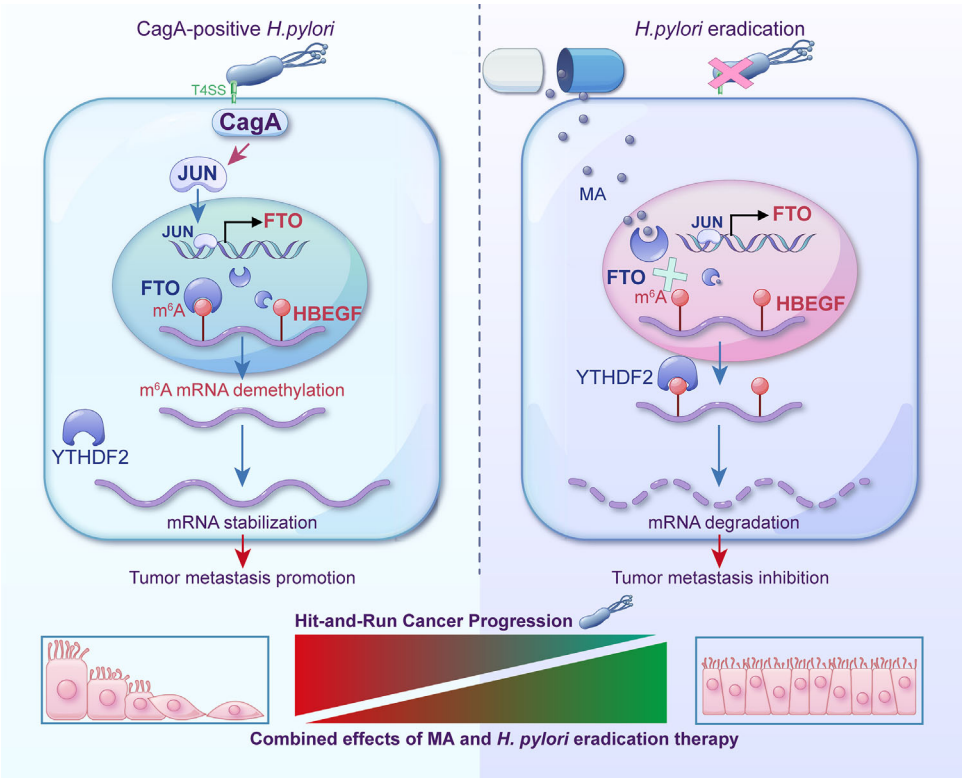

FIGURE 8 Graph illustration. CagA-positive *H. pylori* increases *FTO* expression, which results in "hit-and-run" GC progression. However, the synergism of the *FTO* inhibitor MA with *H. pylori* eradication prevents GC development. Abbreviations: CagA, cytotoxin-associated gene A; CEA, carcinoembryonic antigen; CK20, cytokeratin 20; CK7, cytokeratin 7; EpCAM, epithelial cell adhesion molecule; FTO, fat mass and obesity-associated protein; FTO, fat mass and obesity-associated protein; GAPDH, Glyceraldehyde 3-phosphate dehydrogenase; HBEGF, heparin-binding EGF like growth factor; JUN, Jun Proto-Oncogene; m^6A, N6-methyladenosine; MA, meclofenamic acid; T4SS, the type IV secretion system; YTHDF2, YTH N(6)-methyladenosine RNA binding protein 2.

of EMT is strongly interrelated with tumor metastasis and invasion [51, 53]. It was revealed in our study that *cagA*$^+$ *H. pylori* triggers the EMT process in an FTO-dependent manner. Several EMT-related genes (*HBEGF*, *FKBP5*, *EPB41L3*, *EPHA8*, *PGF*, *KRT18*, *MAGED1*, *PHLDA2*, *WNT3A*, *and TIAM1*) were screened and determined to be regulated by FTO. Among these genes, *HBEGF* is capable of inducing EMT in a variety of epithelial cells [36, 54, 55]. Previous studies had shown that the extracellular domain of HBEGF was cleaved after synthesis, resulting in the shedding of biologically active soluble HBEGF [56]. An increase in secreted HBEGF was shown to induce EMT and promote epithelial cell invasion, whereas membrane-bound HBEGF failed to induce EMT [36–38]. Our findings confirmed that *HBEGF* expression and secretion, determining factors in EMT promotion, were regulated by the CagA-FTO axis.

Clinical evidence is supportive of the continued necessity for *H. pylori* eradication in post-surgical GC patients [12, 13, 15]. However, it has been indicated by several studies that GC progression may persist despite the eradication of *H. pylori* [16, 17]. This finding may stem from the fact that genomic and epigenetic alterations induced by *cagA*$^+$ *H. pylori* infection are not entirely reversed by eradication. The intricate mechanism behind this "hit-and-run" effect remains unclear. Interestingly, it was revealed in our results that CagA was largely eliminated after antibiotic treatment, while the CagA-induced expression of *FTO* and *HBEGF* remained significantly elevated compared to pre-infection levels. This observation was validated through a CagA-tet-on system designed to mimic chronic *cagA*$^+$ *H. pylori* infection. Insights into a possible molecular mechanism for the CagA-induced "hit-and-run" phenomenon were offered by our results, highlighting m^6A modification as a key epigenetic factor. The importance of mitigating the epigenetic changes induced by CagA was underscored by these findings. Consequently, restoring m^6A homeostasis may be a potential therapeutic method for treating GC with *cagA*$^+$ *H. pylori* infection. Satisfactory outcomes have been yielded by preclinical experiments on the discovery of FTO inhibitors [47, 57, 58]. MA, as an FTO-specific inhibitor that does not affect the function of ALKBH5 [41], was previously approved by the FDA for the treatment of osteoarthritis [40]. Guided by these findings, MA was

selected to counteract the effects of CagA-induced *FTO* upregulation. Our data fully confirmed that a combination of MA and antibiotics could significantly impede the progression of GC.

While our study provides evidence that infection with *cagA*$^+$ *H. pylori* may lead to irreversible epigenetic alterations, several limitations warrant discussion. Our findings, initially observed in cell line models, were corroborated using a CagA-tet-on system. However, the generalizability of these results to clinical settings needs further validation through patient-involved interventional studies. Moreover, the mechanisms underlying the epigenetic reprogramming induced by CagA, which appear to be irreversible, require a more comprehensive investigation. Animal studies typically employ models of lung metastasis to assess the metastatic potential of GC [59, 60], employing a broader range of in vivo models could potentially reinforce the conclusions drawn from our experiments. Comorbidities, including preexisting conditions and concurrent infections, may synergistically accelerate the progression of GC [5, 61, 62]. Comprehensively analysis of the role of *H. pylori* infection and these comorbidities in promoting GC progression is required for future studies. Moreover, no studies have linked the use of MA to GC development, although epidemiologic data suggest that NSAID use reduces the incidence of noncardiac GCs [63, 64]. The identification of further studies on the clinical use of MA in GC patients will be interesting because our study confirmed the efficacy of MA in preventing GC progression.

5 | CONCLUSIONS

This study elucidates the molecular mechanism of FTO's role in CagA-promoted GC progression, and provides new evidence that CagA-induced GC progression through a "hit-and-run" mechanism, characterized by irreversible epigenetic changes even after the bacterium's clearance. Our results provide strong evidence for the further clinical exploration of strategies aimed at blocking FTO activity. Such interventions hold promise for halting the CagA-induced "hit-and-run" effects and potentially preventing the progression of GC.

AUTHOR CONTRIBUTIONS

Shiming Yang and Yufeng Xiao designed the project. Bing He, Yiyang Hu, Yuyun Wu, Chao Wang, Limin Gao, Chunli Gong, Zhibin Li, Nannan Gao and Huan Yang performed the experiments. Yufeng Xiao and Bing He analyzed the data and prepared the figures and tables. Bing He, Limin Gao and Chao Wang collected all of the tissue samples. Bing He, Yufeng Xiao and Shiming Yang wrote the manuscript and all of the authors proofed it. Shiming Yang and Yufeng Xiao conceived the project and supervised and coordinated all aspects of the work.

ACKNOWLEDGMENTS

We are grateful to professors Yuan Zhuang and Quanming Zou from Army Military Medical University for supplying the *H. pylori* strains. This project was supported by the National Natural Science Foundation of China (No. 82203479), the Key Program of Natural Science Foundation of Chongqing (No. cstc2020jcyj-zdxmX0020) and the Natural Science Foundation of Chongqing (No. CSTB2023NSCQ-MSX0408).

CONFLICT OF INTEREST STATEMENT

The authors declare that they have no competing interests.

DATA AVAILABILITY STATEMENT

RNA-seq and MeRIP-seq data generated in this study have been deposited in the Genome Sequence Archive database (GSA, https://ngdc.cncb.ac.cn/gsa-human/) under the accession number HRA009431.

ETHICS APPROVAL AND CONSENT TO PARTICIPATE

This study was approved by the Medical Ethics Committee of Xinqiao Hospital of Army Medical University (Approved No. 2024-083-01), and by Shanghai Outdo Biotech Co. Ltd. (Approved No. YBM-05-02). All animal studies were conducted in compliance with protocols approved by the Laboratory Animal Welfare and Ethics Committee of Army Military Medical University (Approved No. AMUWEC20235107).

ORCID

Shiming Yang https://orcid.org/0000-0002-5911-8746

REFERENCES

1. Morgan E, Arnold M, Camargo MC, Gini A, Kunzmann AT, Matsuda T, et al. The current and future incidence and mortality of gastric cancer in 185 countries, 2020-40: A population-based modelling study. EClinicalMedicine. 2022;47:101404.
2. Huang J, Lucero-Prisno DE, Zhang L, Xu W, Wong SH, Ng SC, et al. Updated epidemiology of gastrointestinal cancers in East Asia. Nat Rev Gastroenterol Hepatol. 2023;20(5):271-287.
3. Sharafutdinov I, Tegtmeyer N, Linz B, Rohde M, Vieth M, Tay AC-Y, et al. A single-nucleotide polymorphism in Helicobacter pylori promotes gastric cancer development. Cell Host Microbe. 2023;31(8):1345-1358.
4. Usui Y, Taniyama Y, Endo M, Koyanagi YN, Kasugai Y, Oze I, et al. Helicobacter pylori, Homologous-Recombination Genes, and Gastric Cancer. N Engl J Med. 2023;388(13):1181-1190.
5. Noto JM, Piazuelo MB, Shah SC, Romero-Gallo J, Hart JL, Di C, et al. Iron deficiency linked to altered bile acid metabolism

promotes Helicobacter pylori-induced inflammation-driven gastric carcinogenesis. J Clin Invest. 2022;132(10):e147822.
6. Yamaoka Y. Mechanisms of disease: Helicobacter pylori virulence factors. Nat Rev Gastroenterol Hepatol. 2010;7(11):629-641.
7. Takahashi-Kanemitsu A, Knight CT, Hatakeyama M. Molecular anatomy and pathogenic actions of Helicobacter pylori CagA that underpin gastric carcinogenesis. Cell Mol Immunol. 2020;17(1):50-63.
8. Franco AT, Johnston E, Krishna U, Yamaoka Y, Israel DA, Nagy TA, et al. Regulation of gastric carcinogenesis by Helicobacter pylori virulence factors. Cancer Res. 2008;68(2):379-387.
9. Cao L, Zhu S, Lu H, Soutto M, Bhat N, Chen Z, et al. Helicobacter pylori-induced RASAL2 Through Activation of Nuclear Factor-κB Promotes Gastric Tumorigenesis via β-catenin Signaling Axis. Gastroenterology. 2022;162(6):1716-1731.
10. Palrasu M, Zaika E, El-Rifai W, Garcia-Buitrago M, Piazuelo MB, Wilson KT, et al. Bacterial CagA protein compromises tumor suppressor mechanisms in gastric epithelial cells. J Clin Invest. 2020;130(5):2422-2434.
11. Suzuki G, Cullings H, Fujiwara S, Hattori N, Matsuura S, Hakoda M, et al. Low-positive antibody titer against Helicobacter pylori cytotoxin-associated gene A (CagA) may predict future gastric cancer better than simple seropositivity against H. pylori CagA or against H. pylori. Cancer Epidemiol Biomarkers Prev. 2007;16(6):1224-1228.
12. Li D, Jiang S-F, Lei NY, Shah SC, Corley DA. Effect of Helicobacter pylori Eradication Therapy on the Incidence of Noncardia Gastric Adenocarcinoma in a Large Diverse Population in the United States. Gastroenterology. 2023;165(2):391-401.
13. Ford AC, Yuan Y, Moayyedi P. Long-Term Impact of Helicobacter pylori Eradication Therapy on Gastric Cancer Incidence and Mortality in Healthy Infected Individuals: A Meta-Analysis Beyond 10 Years of Follow-Up. Gastroenterology. 2022;163(3):754-756.
14. Chiang T-H, Chang W-J, Chen SL-S, Yen AM-F, Fann JC-Y, Chiu SY-H, et al. Mass eradication of Helicobacter pylori to reduce gastric cancer incidence and mortality: a long-term cohort study on Matsu Islands. Gut. 2021;70(2):243-250.
15. Yan L, Chen Y, Chen F, Tao T, Hu Z, Wang J, et al. Effect of Helicobacter pylori Eradication on Gastric Cancer Prevention: Updated Report From a Randomized Controlled Trial With 26.5 Years of Follow-up. Gastroenterology. 2022;163(1):154-162.
16. Rokkas T, Pistiolas D, Sechopoulos P, Robotis I, Margantinis G. The long-term impact of Helicobacter pylori eradication on gastric histology: a systematic review and meta-analysis. Helicobacter. 2007;12(Suppl 2):32-8.
17. Chen H-N, Wang Z, Li X, Zhou Z-G. Helicobacter pylori eradication cannot reduce the risk of gastric cancer in patients with intestinal metaplasia and dysplasia: evidence from a meta-analysis. Gastric Cancer. 2016;19(1):166-175.
18. Imai S, Ooki T, Murata-Kamiya N, Komura D, Tahmina K, Wu W, et al. Helicobacter pylori CagA elicits BRCAness to induce genome instability that may underlie bacterial gastric carcinogenesis. Cell Host Microbe. 2021;29(6):941-958.
19. Hatakeyama M. Helicobacter pylori CagA and gastric cancer: a paradigm for hit-and-run carcinogenesis. Cell Host Microbe. 2014;15(3):306-316.
20. Liu Y, You Y, Lu Z, Yang J, Li P, Liu L, et al. N 6-methyladenosine RNA modification-mediated cellular metabolism rewiring inhibits viral replication. Science. 2019;365(6458):1171-1176.
21. Cui Y-H, Yang S, Wei J, Shea CR, Zhong W, Wang F, et al. Autophagy of the m6A mRNA demethylase FTO is impaired by low-level arsenic exposure to promote tumorigenesis. Nat Commun. 2021;12(1):2183.
22. Lin J, Zhan G, Liu J, Maimaitiyiming Y, Deng Z, Li B, et al. YTHDF2-mediated regulations bifurcate BHPF-induced programmed cell deaths. Natl Sci Rev. 2023;10(12):nwad227.
23. Zhai J, Chen H, Wong CC, Peng Y, Gou H, Zhang J, et al. ALKBH5 Drives Immune Suppression Via Targeting AXIN2 to Promote Colorectal Cancer and Is a Target for Boosting Immunotherapy. Gastroenterology. 2023;165(2):445-462.
24. Qing Y, Dong L, Gao L, Li C, Li Y, Han L, et al. R-2-hydroxyglutarate attenuates aerobic glycolysis in leukemia by targeting the FTO/m6A/PFKP/LDHB axis. Mol Cell. 2021;81(5):922-939.
25. Wang L, Dou X, Chen S, Yu X, Huang X, Zhang L, et al. YTHDF2 inhibition potentiates radiotherapy antitumor efficacy. Cancer Cell. 2023;41(7):1294-1308.
26. Hu Y, Gong C, Li Z, Liu J, Chen Y, Huang Y, et al. Demethylase ALKBH5 suppresses invasion of gastric cancer via PKMYT1 m6A modification. Mol Cancer. 2022;21(1):34.
27. Zhang X, Soutto M, Chen Z, Bhat N, Zhu S, Eissmann MF, et al. Induction of Fibroblast Growth Factor Receptor 4 by Helicobacter pylori via Signal Transducer and Activator of Transcription 3 With a Feedforward Activation Loop Involving SRC Signaling in Gastric Cancer. Gastroenterology. 2022;163(3):620-636.
28. Jia G, Fu Y, Zhao X, Dai Q, Zheng G, Yang Y, et al. N6-methyladenosine in nuclear RNA is a major substrate of the obesity-associated FTO. Nat Chem Biol. 2011;7(12):885-887.
29. Chen S, Fan L, Lin Y, Qi Y, Xu C, Ge Q, et al. Bifidobacterium adolescentis orchestrates CD143+ cancer-associated fibroblasts to suppress colorectal tumorigenesis by Wnt signaling-regulated GAS1. Cancer Commun (Lond). 2023;43(9):1027-1047.
30. Shen S, Zhang R, Jiang Y, Li Y, Lin L, Liu Z, et al. Comprehensive analyses of m6A regulators and interactive coding and non-coding RNAs across 32 cancer types. Mol Cancer. 2021;20(1):67.
31. Li Y, Xiao J, Bai J, Tian Y, Qu Y, Chen X, et al. Molecular characterization and clinical relevance of m(6)A regulators across 33 cancer types. Mol Cancer. 2019;18(1):137.
32. Zhou Y, Wang Q, Deng H, Xu B, Zhou Y, Liu J, et al. N6-methyladenosine demethylase FTO promotes growth and metastasis of gastric cancer via m6A modification of caveolin-1 and metabolic regulation of mitochondrial dynamics. Cell Death Dis. 2022;13(1):72.
33. Meyer-ter-Vehn T, Covacci A, Kist M, Pahl HL. Helicobacter pylori activates mitogen-activated protein kinase cascades and induces expression of the proto-oncogenes c-fos and c-jun. J Biol Chem. 2000;275(21):16064-16072.
34. Cristescu R, Lee J, Nebozhyn M, Kim K-M, Ting JC, Wong SS, et al. Molecular analysis of gastric cancer identifies subtypes associated with distinct clinical outcomes. Nat Med. 2015;21(5):449-456.
35. Salt MB, Bandyopadhyay S, McCormick F. Epithelial-to-mesenchymal transition rewires the molecular path to PI3K-dependent proliferation. Cancer Discov. 2014;4(2):186-199.

36. Stoll SW, Rittié L, Johnson JL, Elder JT. Heparin-binding EGF-like growth factor promotes epithelial-mesenchymal transition in human keratinocytes. J Invest Dermatol. 2012;132(9):2148-2157.
37. Yin Y, Grabowska AM, Clarke PA, Whelband E, Robinson K, Argent RH, et al. Helicobacter pylori potentiates epithelial: mesenchymal transition in gastric cancer: links to soluble HB-EGF, gastrin and matrix metalloproteinase-7. Gut. 2010;59(8):1037-1045.
38. Smith JP, Pozzi A, Dhawan P, Singh AB, Harris RC. Soluble HB-EGF induces epithelial-to-mesenchymal transition in inner medullary collecting duct cells by upregulating Snail-2. Am J Physiol Renal Physiol. 2009;296(5): F957-F65.
39. Weng H, Huang F, Yu Z, Chen Z, Prince E, Kang Y, et al. The m6A reader IGF2BP2 regulates glutamine metabolism and represents a therapeutic target in acute myeloid leukemia. Cancer Cell. 2022;40(12):1566-1582.
40. da Costa BR, Pereira TV, Saadat P, Rudnicki M, Iskander SM, Bodmer NS, et al. Effectiveness and safety of non-steroidal anti-inflammatory drugs and opioid treatment for knee and hip osteoarthritis: network meta-analysis. BMJ. 2021;375:n2321.
41. Huang Y, Yan J, Li Q, Li J, Gong S, Zhou H, et al. Meclofenamic acid selectively inhibits FTO demethylation of m6A over ALKBH5. Nucleic Acids Res. 2015;43(1):373-384.
42. Yang L, Kartsonaki C, Yao P, de Martel C, Plummer M, Chapman D, et al. The relative and attributable risks of cardia and non-cardia gastric cancer associated with Helicobacter pylori infection in China: a case-cohort study. Lancet Public Health. 2021;6(12):e888-e96.
43. Malfertheiner P, Camargo MC, El-Omar E, Liou J-M, Peek R, Schulz C, et al. Helicobacter pylori infection. Nat Rev Dis Primers. 2023;9(1):19.
44. Wang J, Yu H, Dong W, Zhang C, Hu M, Ma W, et al. N6-Methyladenosine-Mediated Up-Regulation of FZD10 Regulates Liver Cancer Stem Cells' Properties and Lenvatinib Resistance Through WNT/β-Catenin and Hippo Signaling Pathways. Gastroenterology. 2023;164(6):990-1005.
45. Kim GW, Imam H, Khan M, Mir SA, Kim S-J, Yoon SK, et al. HBV-Induced Increased N6 Methyladenosine Modification of PTEN RNA Affects Innate Immunity and Contributes to HCC. Hepatology. 2021;73(2):533-547.
46. Wang R, Li B, Huang B, Li Y, Liu Q, Lyu Z, et al. Gut Microbiota-Derived Butyrate Induces Epigenetic and Metabolic Reprogramming in Myeloid-Derived Suppressor Cells to Alleviate Primary Biliary Cholangitis. Gastroenterology. 2024; 167(4):733-749.
47. Liu Y, Liang G, Xu H, Dong W, Dong Z, Qiu Z, et al. Tumors exploit FTO-mediated regulation of glycolytic metabolism to evade immune surveillance. Cell Metab. 2021;33(6):1221-1233.
48. Li Z, Weng H, Su R, Weng X, Zuo Z, Li C, et al. FTO Plays an Oncogenic Role in Acute Myeloid Leukemia as a N6-Methyladenosine RNA Demethylase. Cancer Cell. 2017;31(1):127-141.
49. Niu Y, Lin Z, Wan A, Chen H, Liang H, Sun L, et al. RNA N6-methyladenosine demethylase FTO promotes breast tumor progression through inhibiting BNIP3. Mol Cancer. 2019;18(1):46.
50. Zhang J, Bai R, Li M, Ye H, Wu C, Wang C, et al. Excessive miR-25-3p maturation via N6-methyladenosine stimulated by cigarette smoke promotes pancreatic cancer progression. Nat Commun. 2019;10(1):1858.
51. Pastushenko I, Mauri F, Song Y, de Cock F, Meeusen B, Swedlund B, et al. Fat1 deletion promotes hybrid EMT state, tumour stemness and metastasis. Nature. 2021;589(7842):448-455.
52. Yang J, Antin P, Berx G, Blanpain C, Brabletz T, Bronner M, et al. Guidelines and definitions for research on epithelial-mesenchymal transition. Nat Rev Mol Cell Biol. 2020;21(6):341-352.
53. Oh SC, Sohn BH, Cheong J-H, Kim S-B, Lee JE, Park KC, et al. Clinical and genomic landscape of gastric cancer with a mesenchymal phenotype. Nat Commun. 2018;9(1): 1777.
54. Morgan EL, Scarth JA, Patterson MR, Wasson CW, Hemingway GC, Barba-Moreno D, et al. E6-mediated activation of JNK drives EGFR signalling to promote proliferation and viral oncoprotein expression in cervical cancer. Cell Death Differ. 2021;28(5):1669-1687.
55. Cursons J, Leuchowius K-J, Waltham M, Tomaskovic-Crook E, Foroutan M, Bracken CP, et al. Stimulus-dependent differences in signalling regulate epithelial-mesenchymal plasticity and change the effects of drugs in breast cancer cell lines. Cell Commun Signal. 2015;13:26.
56. Luo P, Yan H, Chen X, Zhang Y, Zhao Z, Cao J, et al. s-HBEGF/SIRT1 circuit-dictated crosstalk between vascular endothelial cells and keratinocytes mediates sorafenib-induced hand-foot skin reaction that can be reversed by nicotinamide. Cell Res. 2020;30(9):779-793.
57. Huang Y, Su R, Sheng Y, Dong L, Dong Z, Xu H, et al. Small-Molecule Targeting of Oncogenic FTO Demethylase in Acute Myeloid Leukemia. Cancer Cell. 2019;35(4): 677-691.
58. Su R, Dong L, Li Y, Gao M, Han L, Wunderlich M, et al. Targeting FTO Suppresses Cancer Stem Cell Maintenance and Immune Evasion. Cancer Cell. 2020;38(1):79-96.
59. Zhang L, Li Q, Yang J, Xu P, Xuan Z, Xu J, et al. Cytosolic TGM2 promotes malignant progression in gastric cancer by suppressing the TRIM21-mediated ubiquitination/degradation of STAT1 in a GTP binding-dependent modality. Cancer Commun (Lond). 2023;43(1):123-149.
60. Li S, Guo D, Sun Q, Zhang L, Cui Y, Liu M, et al. MAPK4 silencing in gastric cancer drives liver metastasis by positive feedback between cancer cells and macrophages. Exp Mol Med. 2023;55(2):457-469.
61. Wang G, Wang H, Ji X, Wang T, Zhang Y, Jiang W, et al. Intratumoral microbiome is associated with gastric cancer prognosis and therapy efficacy. Gut Microbes. 2024;16(1):2369336.
62. Zeng R, Gou H, Lau HCH, Yu J. Stomach microbiota in gastric cancer development and clinical implications. Gut. 2024;73(12):2062-2073.
63. Wang WH, Huang JQ, Zheng GF, Lam SK, Karlberg J, Wong BC-Y. Non-steroidal anti-inflammatory drug use and the risk of gastric cancer: a systematic review and meta-analysis. J Natl Cancer Inst. 2003;95(23):1784-1791.
64. Cao Y, Nishihara R, Wu K, Wang M, Ogino S, Willett WC, et al. Population-wide Impact of Long-term Use of Aspirin and the Risk for Cancer. JAMA Oncol. 2016;2(6):762-769.

SUPPORTING INFORMATION

Additional supporting information can be found online in the Supporting Information section at the end of this article.

How to cite this article: He B, Hu Y, Wu Y, Wang C, Gao L, Gong C, et al. *Helicobacter pylori* CagA elevates FTO to induce gastric cancer progression via a "hit-and-run" paradigm. Cancer Commun. 2025;45:608–631. https://doi.org/10.1002/cac2.70004